

Autophagy



ISSN: (Print) (Online) Journal homepage: <https://www.tandfonline.com/loi/kaup20>

Autophagic degradation of KAT2A/GCN5 promotes directional migration of vascular smooth muscle cells by reducing TUBA/ α -tubulin acetylation

Changhan Ouyang , Jing Mu , Qiulun Lu , Jian Li , Huaiping Zhu , Qilong Wang , Ming-Hui Zou & Zhonglin Xie

To cite this article: Changhan Ouyang , Jing Mu , Qiulun Lu , Jian Li , Huaiping Zhu , Qilong Wang , Ming-Hui Zou & Zhonglin Xie (2020) Autophagic degradation of KAT2A/GCN5 promotes directional migration of vascular smooth muscle cells by reducing TUBA/ α -tubulin acetylation, *Autophagy*, 16:10, 1753-1770, DOI: [10.1080/15548627.2019.1707488](https://doi.org/10.1080/15548627.2019.1707488)

To link to this article: <https://doi.org/10.1080/15548627.2019.1707488>



View supplementary material [↗](#)



Published online: 27 Dec 2019.



Submit your article to this journal [↗](#)



Article views: 544



View related articles [↗](#)



View Crossmark data [↗](#)



Citing articles: 2 View citing articles [↗](#)

RESEARCH PAPER



Autophagic degradation of KAT2A/GCN5 promotes directional migration of vascular smooth muscle cells by reducing TUBA/ α -tubulin acetylation

Changhan Ouyang*, Jing Mu*, Qiulun Lu, Jian Li, Huaiping Zhu, Qilong Wang, Ming-Hui Zou, and Zhonglin Xie

Center of Molecular and Translational Medicine, Georgia State University, Atlanta, GA, USA

ABSTRACT

Macroautophagy/autophagy, a fundamental process for degradation of macromolecules and organelles, occurs constitutively at a basal level and is upregulated in response to stress. Whether autophagy regulates protein acetylation and microtubule stability in vascular smooth muscle cells (VSMCs) migration, however, remains unknown. Here, we demonstrate that the histone acetyltransferase KAT2A/GCN5 (lysine acetyltransferase 2) binds directly to the autophagosome protein MAP1LC3/LC3 (microtubule associated protein 1 light chain 3) via a conserved LC3-interacting region (LIR) domain. This interaction is required for KAT2A sequestration in autophagosomes and degradation by lysosomal acid hydrolases. Suppression of autophagy results in KAT2A accumulation. KAT2A functions as an acetyltransferase to increase TUBA/ α -tubulin acetylation, promote microtubule polymerization and stability, ultimately inhibiting directional cell migration. Our findings indicate that deacetylation of TUBA and perturbation of microtubule stability via selective autophagic degradation of KAT2A are essential for autophagy-promoting VSMC migration.

Abbreviations: ACTB: actin beta; ATAT1: alpha tubulin acetyltransferase 1; ATG: autophagy-related; BECN1: beclin 1; CQ: chloroquine; FBS: fetal bovine serum; GST: glutathione S-transferase; H4K16ac: histone H4 lysine 16 acetylation; HASMCs: human aortic smooth muscle cells; HBSS: Hank's buffered salt solution; HDAC6: histone deacetylase 6; hMOF: human males absent on the first; IP: immunoprecipitation; KAT2A/GCN5: lysine acetyltransferase 2A; Lacta: lactacystin; LIR: LC3-interaction region; MAP1LC3: microtubule associated protein 1 light chain 3; MEFs: mouse embryonic fibroblasts; MTOC: microtubule-organizing center; PE: phosphatidylethanolamine; PtdIns3K: class III phosphatidylinositol 3-kinase; RUNX2: runt-related transcription factor 2; SIRT1: sirtuin 1; SIRT2: sirtuin 2; SQSTM1/p62: sequestosome 1; ULK1: unc-51 like autophagy activating kinase 1; VSMCs: vascular smooth muscle cells; WT: wild-type.

ARTICLE HISTORY

Received 2 May 2019
Revised 9 December 2019
Accepted 16 December 2019

KEYWORDS





Autophagy; KAT2A/GCN5; microtubule; TUBA/ α -tubulin; VSMCs

Introduction


Cell migration is a central process in the development and maintenance of multicellular organisms. In an adult organism, cell migration is involved in tissue renewal, immune response, and wound repair, and aberrant cell migration is found in various pathologies, including vascular disease, chronic inflammatory diseases, and tumor metastasis. In the vasculature, migration of vascular smooth muscle cells (VSMCs) from the media to intima occurs during the development of intimal hyperplasia and atherosclerosis [1,2]. Microtubules are essential components of the cytoskeleton and play a major role in cell migration [3]. These polarized polymers are composed of α - and β -Tubulin. Microtubules alternate between phases of growth and shrinkage in a manner described as dynamic instability [4]. Maintaining the balance between dynamically unstable and stable microtubules is required for cell migration. Microtubule stability is regulated by various microtubule-associated proteins and posttranslational modifications, including acetylation, polyglutamylation, and detyrosination. These modifications appear to fine-tune the properties of tubulin and microtubules to facilitate their diverse

functions. Acetylation of microtubules in mammalian cells is positively regulated by a variety of acetyltransferases, including, but not limited to, ATAT1 (alpha tubulin acetyltransferase 1) and the elongator protein complex [5,6]. To date, the histone deacetylase (HDAC) family member HDAC6 (histone deacetylase 6) and SIRT2 (sirtuin 2) are the only TUBA deacetylases to be described [7,8]; however, the enzymes that are responsible for regulating tubulin acetylation and deacetylation in VSMCs remain unknown. Although acetylation of TUBA is always associated with stable microtubules, the precise role of TUBA acetylation in the regulation of microtubule dynamics and cell migration in VSMCs has not been resolved.

Autophagy is a catabolic process that plays a pivotal role in metabolism, cell death, and differentiation [9,10]. During autophagy, cytoplasmic components, including long-lived proteins and organelles, are engulfed by a double-membrane structure and targeted for destruction in lysosomes [11]. Autophagy initiation requires the activation of ULK1 (unc-51 like autophagy activating kinase 1) and the class III phosphatidylinositol 3-kinase (PtdIns3K)-BECN1 (beclin 1)

CONTACT Zhonglin Xie  zxie@gsu.edu  Center for Molecular and Translational Medicine, Georgia State University, 157 Decatur Street North East, Atlanta, GA, USA; Ming-Hui Zou  mzou@gsu.edu  Center for Molecular and Translational Medicine, Georgia State University, 157 Decatur Street North East, Atlanta, GA, USA

*These authors contributed equally to this work.

 Supplemental data for this article can be accessed [here](#).

© 2019 Informa UK Limited, trading as Taylor & Francis Group

complex. Once activated, the ULK1 complex drives initiation of autophagosome formation. Elongation and maturation of autophagosomes are regulated by two well-conserved conjugation systems, the conjugation of ATG12 to ATG5 with the help of ATG7 and ATG10 and the conjugation of phosphatidylethanolamine (PE) to MAP1LC3/LC3/Atg8 (microtubule-associated protein 1 light chain 3) by the sequential action of ATG4, ATG7, and ATG3 [12]. The autophagosome then fuses with the lysosome forming autolysosomes within which the cargos are degraded by lysosomal acid hydrolases [11].

Recently, specific autophagic degradation of polyubiquitinated protein aggregates was described, and this substrate-specific autophagy also regulates the turnover of small molecules and entire organelles within cells [13]. Many studies have shown that autophagy can be regulated by protein acetylation [14], but whether autophagy can regulate protein acetylation remains unknown. Alterations in autophagy activity have been reported in numerous vascular diseases including pulmonary hypertension [15], vascular aging [16], atherosclerosis [17], and restenosis [18]. However, further investigation is required to delineate the mechanism by which autophagy regulates microtubule stability and cell migration and determine the roles of autophagy in vascular diseases. In this study, we demonstrate that activation of autophagy selectively degrades KAT2A, a histone acetyltransferase that acetylates TUBA in VSMCs, leading to microtubule instability and promotion of VSMC migration.

Results

Suppression of autophagy increases TUBA acetylation

Starvation-induced autophagy in mouse embryonic fibroblasts (MEFs) is coupled to reduction of histone H4 lysine 16 acetylation (H4K16ac) [19], prompting us to investigate whether autophagy regulates protein acetylation. We first analyzed the protein acetylation profile in wild-type (WT) MEFs as well as in MEFs deficient for key autophagy genes (*atg5*^{-/-} and *atg7*^{-/-} MEFs) [20,21]. Defective autophagy was verified in *atg5*^{-/-} and *atg7*^{-/-} MEFs, as evidenced by both reduced conversion of LC3-I to LC3-II (a phosphatidylethanolamine derivative of LC3-I) and increased SQSTM1/p62 (sequestosome 1) (a receptor for cargo destined to be degraded by autophagy) levels (Figure S1A). The suppression of autophagy was associated with higher levels of acetylated proteins (Figure 1A).

We further determined whether activation of autophagy reduces protein acetylation by starvation of MEFs with Hank's buffered salt solution (HBSS) (Figure S1b), which is typically used as a trigger of autophagy [22]. Starvation significantly increased the conversion of LC3-I to LC3-II and reduced SQSTM1 levels (Figure S1B), indicating activation of autophagy. This increase in autophagy was accompanied by significant reduction in acetylated protein levels (Figure 1B).

To determine whether autophagy regulates protein acetylation in non-MEF cells such as VSMCs, we examined protein acetylation in human aortic smooth muscle cells (HASMCs). In line with our findings in MEFs, gene silencing of either *ATG5* or *ATG7* suppressed autophagy by reducing LC3-II levels and increasing SQSTM1 levels (Figure S1C), while

concomitantly elevating levels of acetylated proteins (Figure 1C). Conversely, activation of autophagy by starvation (HBSS treatment) increased conversion of LC3-I to LC3-II and reduced SQSTM1 levels (Figure S1D), in concurrence with significant reduction in acetylated protein levels (Figure 1D).

We noted a band with a molecular weight of ~50 KD that was significantly increased in autophagy-deficient cells (Figure 1A, C). In contrast, this protein was reduced in MEFs and HASMCs upon activation of autophagy (Figure 1B, D). Given that a 51-KD TUBA species has been reported to be acetylated and associated with microtubule stability and cell motility [8], we examined whether inhibition of autophagy promotes the acetylation of TUBA. Using an antibody against acetylated-TUBA (anti-TUBA [acetyl K40] antibody [6-11B-1]), we observed that acetylation of TUBA significantly increased in autophagy-deficient *atg5*^{-/-} and *atg7*^{-/-} MEFs (Figure 1E). Similarly, suppression of autophagy in HASMCs by gene silencing of either *ATG5* or *ATG7* also enhanced the levels of acetylated TUBA (Figure 1G). On the contrary, activation of autophagy by starvation reduced acetylated TUBA levels in both MEFs and HASMCs (Figure 1F, H).

Since autophagy can occur through either the ATG5/ATG7-dependent conventional pathway or the ATG5/ATG7-independent alternative pathway [23], we further explored our hypothesis that autophagy regulates acetylation following inhibition of autophagy using siRNA against *BECN1* and *ULK1*, two proteins that are required for the activation of autophagy through either ATG5/ATG7-dependent or ATG5/ATG7-independent pathway [23]. Suppression of autophagy by silencing either *BECN1* or *ULK1* (Figure S1E, F) also increased acetylated TUBA levels (Figure 1I, J). Collectively, these data indicate that autophagy negatively regulates TUBA acetylation.

Inhibition of autophagy increases KAT2A protein expression

To gain insight into the mechanisms by which autophagy regulates TUBA acetylation, we examined whether autophagy regulates the expression of acetyltransferases, KAT2A, KAT8/hMOF (lysine acetyltransferase 8), EP300, ATAT1, and deacetylases (HDAC6, SIRT1, and SIRT2) in HASMCs. Transfection of HASMCs with *ATG5*, *ATG7*, *BECN1*, or *ULK1* siRNA resulted in lower levels of ATG5, ATG7, BECN1, or ULK1 respectively, inhibited the conversion of LC3-I to LC3-II, and increased SQSTM1 protein level (Figures S1C–F, S2A). Suppression of autophagy was associated with an increase in KAT2A protein levels (Figures 2A–C, S2A, B), but the suppression of autophagy by *ULK1* siRNA did not affect the expression of ATAT1, KAT8, EP300, HDAC6, SIRT1 or SIRT2 (Figure S2B).

Next, we determined if autophagy activation by HBSS treatment leads to changed expression of any HDACs including ATAT1, KAT8, EP300, SIRT1 or SIRT2. Activation of autophagy reduced KAT2A protein level but has no effects on the expression of ATAT1, KAT8, EP300, SIRT1, and SIRT2 (Figure S2C). We also examined the expression of other HDACs, including HDAC4, HDAC5, HDAC6, HDAC7, and HDAC9, in the autophagy activation (HBSS

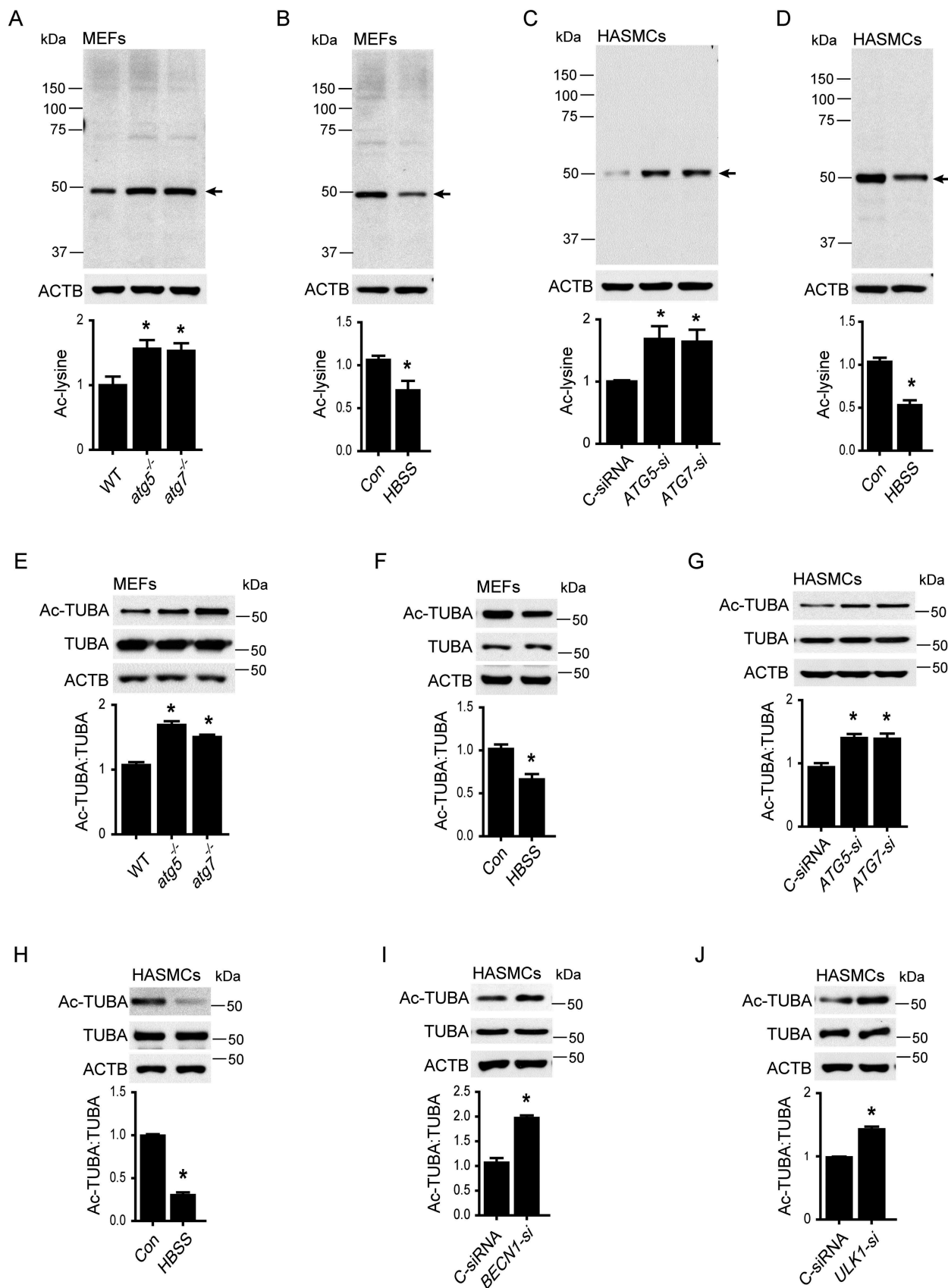


Figure 1. Autophagy regulates TUBA acetylation. (A) Western blot analysis of protein acetylation in wild-type (WT), *atg5*^{-/-}, and *atg7*^{-/-} mouse embryonic fibroblasts (MEFs). $n = 5$, $*P < 0.05$ vs. WT. (B) WT MEFs were starved with Hank's balanced salt solution (HBSS) for 3 h, and acetylated proteins were analyzed by western blotting. $n = 5$, $*P < 0.05$ vs. control (con). (C) Human aortic smooth muscle cells (HASMCs) were transfected with control siRNA (C-siRNA) or siRNA targeting *ATG5* (ATG5-si) or *ATG7* (ATG7-si) for 48 h. Protein acetylation was measured by western blotting. $n = 5$, $*P < 0.05$ vs. C-siRNA. (D) HASMCs were starved with HBSS for 3 h. Protein acetylation was analyzed by western blot. $n = 5$, $*P < 0.05$ vs. Con. (E) Western blot analysis of acetylation of TUBA (Ac-TUBA) in WT, *atg5*^{-/-}, and *atg7*^{-/-} MEFs. $n = 5$, $*P < 0.05$ vs. WT. (F) Western blot analysis of Ac-TUBA in MEFs subjected to starvation. $n = 5$, $*P < 0.05$ vs. Con. (G) Levels of Ac-TUBA were determined by western blot in HASMCs transfected with C-siRNA, *ATG5* siRNA, or *ATG7* siRNA. $n = 5$, $*P < 0.05$ vs. C-siRNA. (H) Western blot analysis of Ac-TUBA in HASMCs subjected to starvation. $n = 5$, $*P < 0.05$ vs. Con. (I) Western blots detected the indicated proteins in HASMCs transfected with C-siRNA or *BECN1* siRNA (*BECN1*-si). $n = 5$, $*P < 0.05$ vs. C-siRNA. (J) Western blot analysis of Ac-TUBA in HASMCs transfected with C-siRNA or *ULK1* siRNA (*ULK1*-si). $n = 5$, $*P < 0.05$ vs. C-siRNA.

treatment) condition. The activation of autophagy did not alter the expression of these HDACs either (Figure S2D).

We further validated the effect of autophagy on KAT2A expression in WT, *atg5*^{-/-}, and *atg7*^{-/-} MEFs and found that deletion of either *Atg5* or *Atg7* significantly increased KAT2A protein expression (Figure 2E–G). Notably, defective autophagy had no effect on KAT2A mRNA expression (Figure 2D, H), suggesting that autophagy regulates KAT2A at the posttranslational level. Conversely, adenovirus overexpression of either ATG5 or ATG7 increased conversion of LC3-I to LC3-II (Figure 2I, K) and reduced SQSTM1 levels (Figure S2E, H), in concurrence with significant reduction in KAT2A protein levels (Figure 2I, J).

We further examined whether activation of autophagy by starvation increases KAT2A degradation in WT and *atg5*^{-/-} MEFs. As expected, starvation (HBSS treatment) activated autophagy as evidenced by increased LC3-II to LC3-I ratios in WT MEFs (Figure 2L, M), and HBSS treatments failed to activate autophagy in *atg5*^{-/-} MEFs (Figure 2L, M). As autophagy was activated in WT MEFs, KAT2A protein levels declined gradually (Figure 2I, N). More specifically, KAT2A was reduced by 50% in these cells after 24 h HBSS treatment (Figure 2I, N). In contrast, in autophagy-defective *atg5*^{-/-} MEFs, HBSS treatment did not alter KAT2A levels compared to levels in the vehicle-treated cells (Figure 2I, N), indicating KAT2A protein degradation by autophagy was inhibited in *atg5*^{-/-} MEFs. Similarly, starvation also promoted the degradation of exogenous KAT2A in HeLa cells, because following transfection of HeLa cells with *GFP* or *Flag-KAT2A* plasmid and subsequent starvation by incubation of the cells in HBSS, KAT2A levels were decreased in a time-dependent manner (Figure 2O). Taken together, autophagy activation promotes KAT2A protein degradation.

To investigate whether the proteasome is involved in this KAT2A degradation, we treated HASMCs with the lysosome inhibitor chloroquine (CQ) [24] or the proteasome inhibitor lactacystin (Lacta) [25]. CQ treatment resulted in increased levels of LC3-II and SQSTM1 proteins (inhibition of autophagic flux) in association with an increase in the KAT2A protein level (Figure 2P), indicating that defective autophagy reduces KAT2A protein degradation. Conversely, proteasome inhibition with Lacta, which exerts no effect on autophagy activity, increased protein level of RUNX2 (runt related transcription factor 2), a well-known protein degraded by proteasomal pathway [26], but failed to alter KAT2A protein levels (Figure 2P). Taken together, these data suggest that KAT2A is degraded through the autophagy-lysosomal pathway.

KAT2A binds to LC3 and co-localizes with autophagosomes

To confirm our results that suggest autophagic degradation of KAT2A, we examined the localization of KAT2A in autophagosomes using immunostaining of KAT2A in HASMCs transfected with *GFP-LC3* adenovirus as a probe for detection of autophagosome formation. Fluorescence microscopy analysis revealed that KAT2A (red) was not only localized in the nucleus but was also distributed in the cytoplasm. Interestingly, some of the KAT2A protein in the cytoplasm

co-localized with GFP-LC3 puncta (Figure 3A). The co-localization of KAT2A and LC3 suggests that these two proteins may interact physiologically with each other.

To test this possibility, we first examined the interaction between KAT2A and LC3 in HeLa cells transfected with *EGFP* or *EGFP-LC3* plasmid. Twenty-four h after transfection, cells were collected for immunoprecipitation (IP) with anti-KAT2A antibody and immunoblotting with GFP antibody. A band representing GFP-LC3 was detected in the cells transfected with *EGFP-LC3* and immunoprecipitated with anti-KAT2A but not in the cells transfected with *GFP* (Figure 3B). In addition, glutathione S-transferase (GST)-LC3 beads pulled down recombinant full-length KAT2A in binding buffer (Figure 3C), indicating that KAT2A physically associates with LC3 in cells.

We next determined whether SQSTM1 mediates the interaction between KAT2A and LC3. In HeLa cells, ectopically overexpressed MYC-LC3 associated with endogenous KAT2A (Figure 3D); however, overexpressed Flag-KAT2A did not associate with SQSTM1 (Figure 3E). Importantly, gene silencing of *SQSTM1* did not disrupt the association between KAT2A and LC3 in HeLa cells, (Figure S3), suggesting that KAT2A physically interacts with LC3, and SQSTM1 is not involved in the interaction between KAT2A and LC3.

The LC3 interaction region (LIR) domain of KAT2A mediates the association of KAT2A with LC3 and is essential for KAT2A degradation

Next, we investigated whether the LIR domain of KAT2A is required for KAT2A degradation. Autophagy receptor proteins, such as NBR1 (NBR1 autophagy cargo receptor), SQSTM1, Atg32, and FUNDC1 (FUN14 domain containing 1), bind to LC3 and LC3 homologues through an LIR domain that is typified by the core consensus sequence W/F/YxxL/I/V (Figure S4A) [27,28]. To determine whether KAT2A is an autophagy substrate, we analyzed KAT2A protein sequence for predicted LIR domains and found four candidate LIR domains in KAT2A at amino acids 661–664, 716–719, 734–737, and 826–829 (Figure S4B). To investigate whether one of these LIR domains mediates the interaction between KAT2A and LC3 and to identify which one, we generated a series of LIR domain deletion mutants (Figure S4C). These mutants were overexpressed in HEK293 cells, and the interaction between KAT2A and endogenous LC3 was determined by immunoprecipitation and western blotting. As depicted in Figure 3F, the mutant with deletion of amino acids 734–737, but not mutants with deletion of the other candidate domains at amino acids 661–664, 716–719, and 826–829, completely disrupted the interaction between KAT2A and LC3. To further demonstrate that KAT2A interacts with LC3 through the LIR (734–737), we mutated Y734 and L737 to alanine and overexpressed this mutant in HeLa cells. Immunoprecipitation and western blotting showed that altering the sequence at the LIR also completely prevented the interactions between KAT2A and LC3 (Figure 3G), indicating that amino acids 734–737 comprise the LIR domain that mediates the interaction between KAT2A and LC3.

To determine whether this KAT2A LIR domain is required for KAT2A degradation by autophagy, we expressed WT KAT2A or mutant KAT2A (734–737 deletion) in HEK293

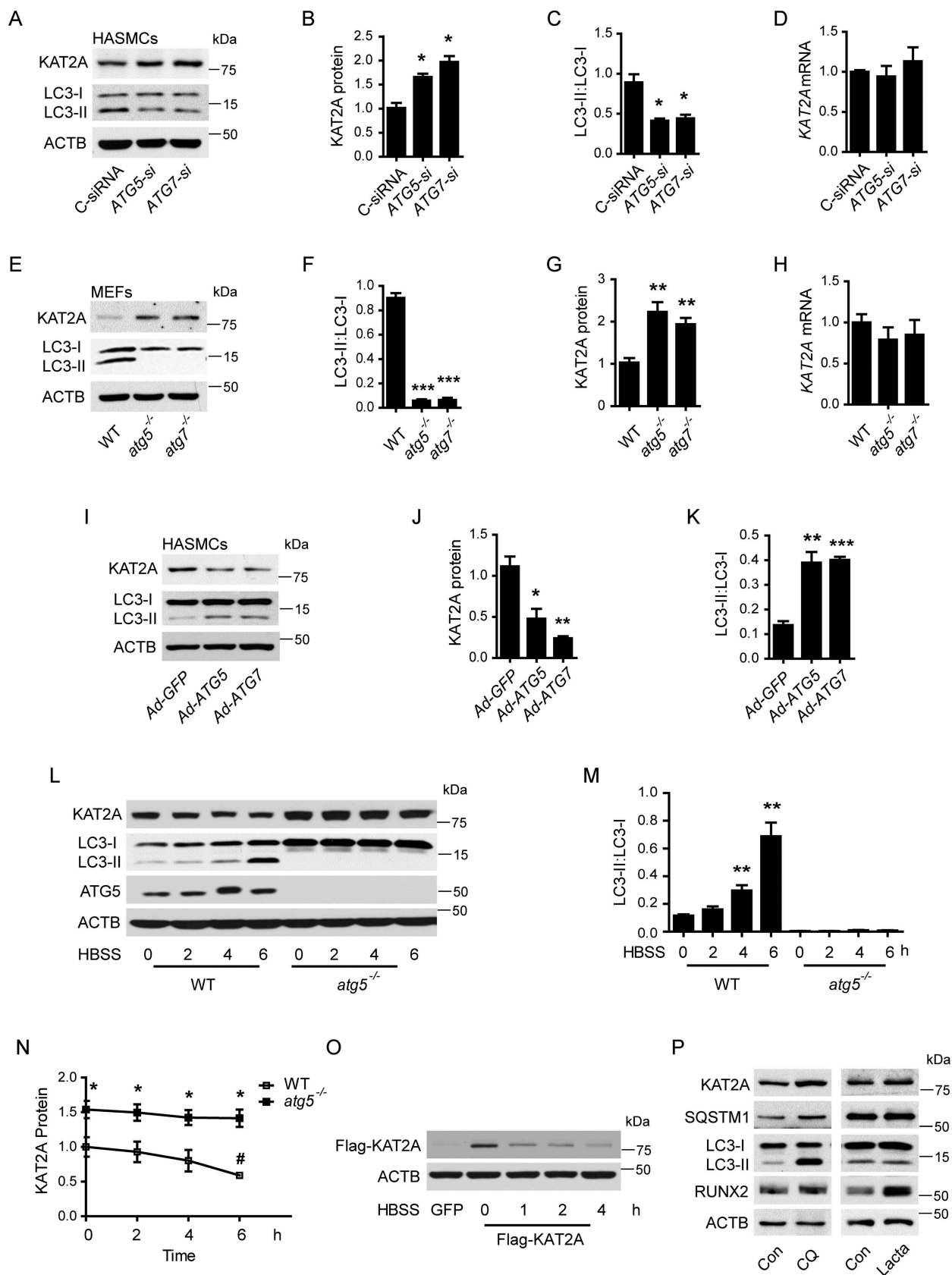


Figure 2. Autophagy inhibition increases KAT2A protein levels. (A–C) HASMCs were transfected with control siRNA (C-siRNA), ATG5 siRNA (ATG5-si), or ATG7 siRNA (ATG7-si) for 48 h. Protein levels of KAT2A and LC3-I or LC3-II were analyzed by western blotting and densitometry. $n = 3$, $*P < 0.05$ vs. C-siRNA. (D) KAT2A mRNA was measured by quantitative real-time PCR. (E–G) Western blot and densitometry analysis of KAT2A and LC3-I or LC3-II protein levels in WT, *atg5*^{-/-}, and *atg7*^{-/-} MEFs. $n = 3$, $**P < 0.01$ vs. WT, $***P < 0.001$ vs. WT. (H) Expression of KAT2A mRNA in WT, *atg5*^{-/-}, and *atg7*^{-/-} MEFs. (I–K) HASMCs were transfected with Ad-GFP, Ad-ATG5, or Ad-ATG7 for 48 h. Protein levels of KAT2A and LC3-I or LC3-II were evaluated by western blotting and densitometry. $n = 3$, $*P < 0.05$, $**P < 0.01$, $***P < 0.001$ vs. ad-GFP. (L) WT and *atg5*^{-/-} MEFs were starved with HBSS for the indicated time points. Protein levels of KAT2A, LC3-I or LC3-II, and ATG5 were analyzed by western blotting. (M) The LC3-II to LC3-I ratio was analyzed by densitometry. $n = 3$, $***P < 0.001$ vs. control. (N) KAT2A degradation was analyzed by densitometry. $n = 3$, $*P < 0.05$ vs. *atg5*^{-/-} MEFs; $#P < 0.05$ vs. *atg5*^{-/-} 0 h. (O) HeLa cells were transfected with plasmid encoding GFP or Flag-KAT2A for 48 h and then starved with HBSS for the indicated time points. Expression of Flag-KAT2A was determined by western blotting. (P) HASMCs were treated with chloroquine (CQ, 10 μ M) or lactacystin (Lacta, 5 μ M) for 24 h. Levels of KAT2A, SQSTM1, LC3-I or LC3-II and RUNX2 were analyzed by western blotting.

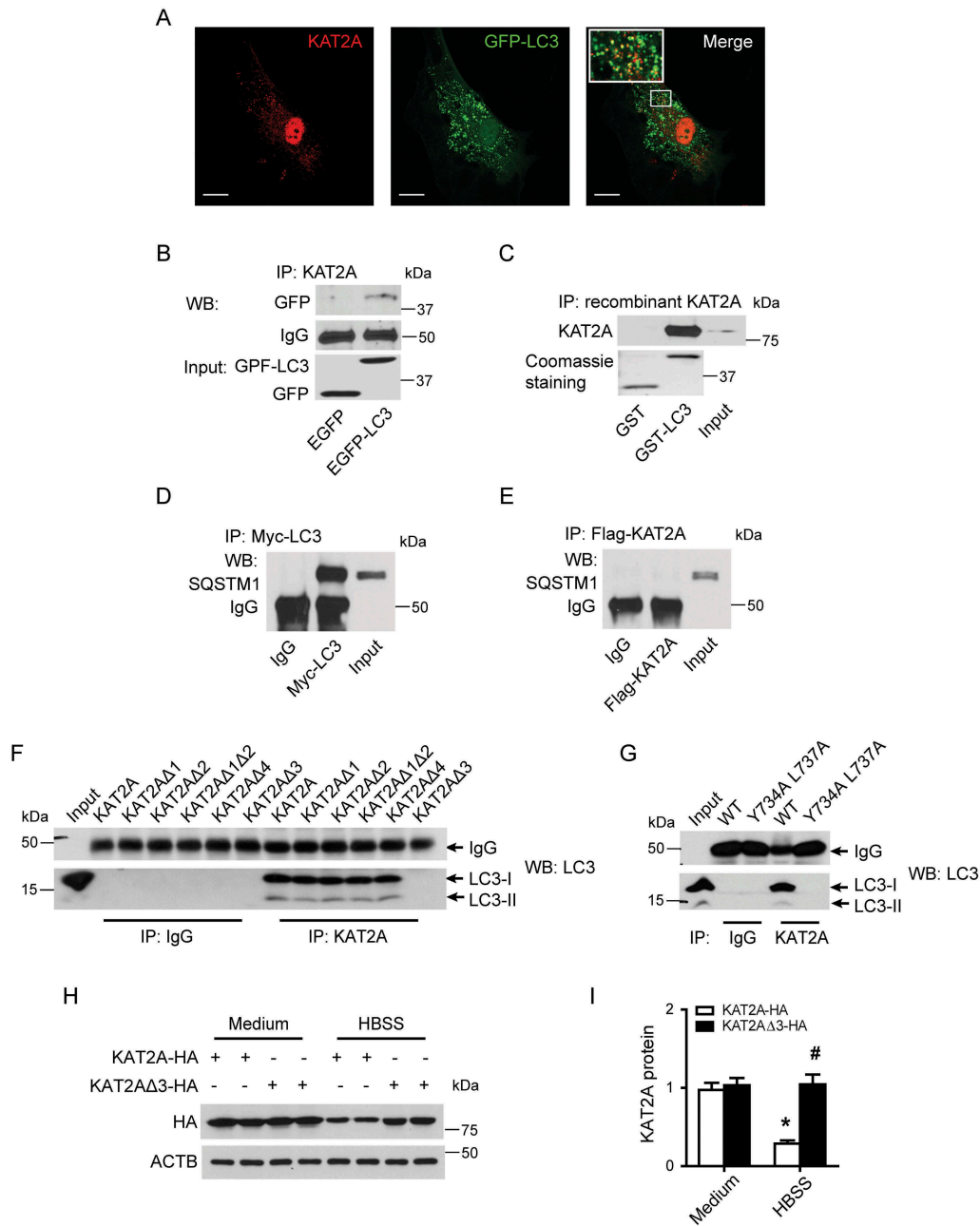


Figure 3. KAT2A is degraded through the autophagic-lysosomal pathway. (A) HASMCs were transfected with an adenovirus encoding GFP-LC3 for 24 h and then treated with chloroquine for 16 h. KAT2A was stained by immunocytochemistry, and the co-localization (yellow) of KAT2A (red) and GFP-LC3 puncta was evaluated by immunofluorescence microscopy. Scale bar: 20 μ m. (B) HeLa cells were transfected with EGFP or EGFP-LC3 plasmid for 24 h. The interaction between KAT2A and LC3B was determined by immunoprecipitation (IP) of KAT2A and subsequent western blotting (WB) with GFP. (C) Recombinant full-length KAT2A was incubated with GST- or GST-LC3-immobilized beads and then subjected to SDS-PAGE. KAT2A was detected with KAT2A antibody. Coomassie staining was used to visualize GST and GST-LC3 proteins. (D) HeLa cells were transfected with plasmid encoding MYC-LC3 for 48 h, and the interaction between LC3 and SQSTM1 was determined by IP and WB as indicated. (E) HeLa cells were transfected with plasmid encoding Flag-KAT2A for 48 h, and the interaction between KAT2A and SQSTM1 was determined by IP and WB as indicated. (F) HeLa cells were transfected with the indicated KAT2A constructs for 24 h. Cell lysates were immunoprecipitated using IgG or KAT2A antibody, and LC3B antibody was used for WB. (G) HeLa cells were transfected with plasmids encoding WT and KAT2A^{Y734A, L737A} mutant for 24 h. Cells were lysed and immunoprecipitated using IgG or KAT2A antibody. The immunoprecipitated proteins were detected by western blotting with LC3B antibody. (H and I) HeLa cells were transfected with WT or KAT2A^{Y734A, L737A} mutant for 48 h and then starved with incubation in HBSS for 3 h to activate autophagy. KAT2A protein levels were analyzed by WB and densitometry. $n = 3$, *** $P < 0.001$ vs. KAT2A-HA/Medium; ### $P < 0.001$ vs. KAT2A-HA/HBSS.

cells. After transfection, the cells were subjected to starvation with HBSS. As depicted in Figure 3H, I, activation of autophagy reduced WT KAT2A protein levels. Deletion of the LIR domain of KAT2A amino acids 734–737 abrogated this KAT2A reduction induced by autophagy activation (Figure 3H, I). Thus, the LIR domain at amino acids 734–737 of KAT2A is required for KAT2A autophagic degradation.

KAT2A induces TUBA acetylation

To investigate whether KAT2A acetylates TUBA, we first examined whether KAT2A interacts with TUBA in WT and *atg5*^{-/-} MEFs. Immunoprecipitation and western blot analysis demonstrated that KAT2A associated with TUBA in WT MEFs, and this association was enhanced in autophagy-

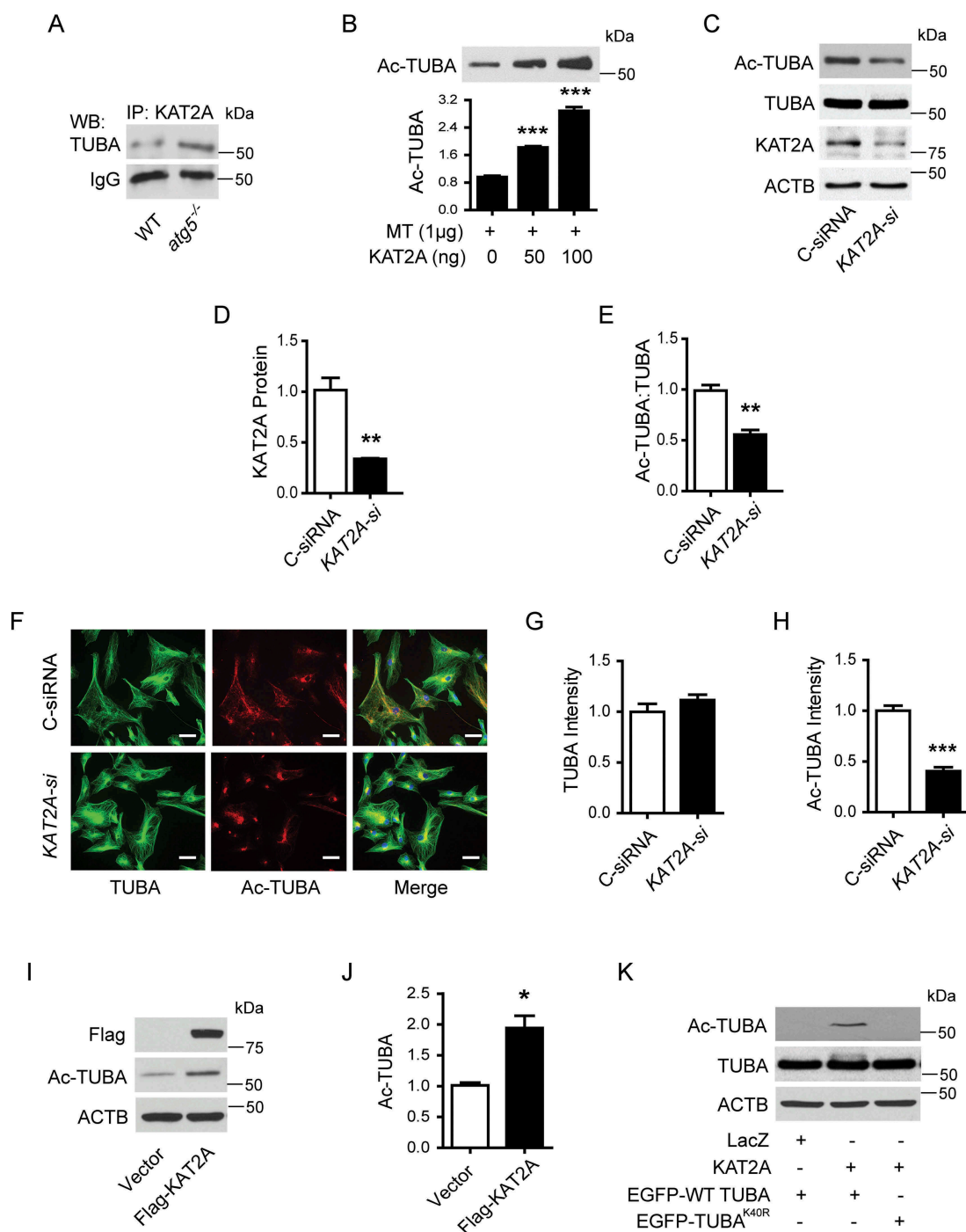


Figure 4. KAT2A acetylates TUBA. (A) The interaction of KAT2A and TUBA in *atg5*^{-/-} MEFs was determined by immunoprecipitation and western blotting. (B) Purified porcine brain tubulin protein was incubated with recombinant KAT2A-catalytic domain protein in acetylation buffer at 37°C for 1 h. The acetylation of TUBA (Ac-tubulin) was assessed by western blotting. $n = 3$, $***P < 0.001$. (C-E) HASMCs were transfected with control siRNA (C-siRNA) or KAT2A siRNA (KAT2A-si). Expression of KAT2A and acetylation of TUBA were examined by western blot and densitometry. $n = 3$, $**P < 0.01$. (F-H) HASMCs were transfected with control siRNA (C-siRNA) or KAT2A siRNA (KAT2A-si). Acetylation of TUBA was analyzed by immunofluorescence. Scale bar: 50 μm . $n = 3$, $***P < 0.001$. (I and J) HEK 293 cells were transfected with a plasmid encoding Flag-KAT2A for 48 h. Acetylation of TUBA was assayed by western blotting and densitometry. $n = 3$, $*P < 0.01$. (K) HEK293 cells were co-transfected with plasmid encoding LacZ, KAT2A, EGFP-WT-TUBA, or EGFP-TUBA^{K40R} for 48 h. Acetylation of TUBA was examined by western blotting.

deficient *atg5*^{-/-} MEFs, due to the accumulation of KAT2A in the cells (Figure 4A), indicating that KAT2A specifically interacts with TUBA. Next, we examined whether KAT2A directly acetylates TUBA in a cell free system by incubating purified porcine brain tubulin protein (>99% pure) with recombinant KAT2A-catalytic domain protein in acetylation buffer, we

found that the KAT2A-catalytic domain alone was sufficient to induce TUBA acetylation, as evidenced by increased acetylated TUBA in the purified porcine brain tubulin protein in a dose-dependent manner (Figure 4B).

We further examined whether KAT2A induces TUBA acetylation in HASMCs using gain-of- and loss-of-function

approaches. As depicted in Figure 4C–E, the transfection of *KAT2A* siRNA dramatically reduced *KAT2A* protein levels as well as levels of TUBA acetylation (Figure 4C–E). Immunofluorescence analysis confirmed that *KAT2A* gene silencing reduced the levels of acetylated TUBA (Figure 4F–H). In contrast, ectopic expression of *KAT2A* in HEK 293 cells resulted in increased levels of acetylated TUBA (Figure 4I, J).

To date, the most-studied modification of tubulin is acetylation of Lys40 (K40) of TUBA [29]. Therefore, we examined whether *KAT2A* induces acetylation of TUBA specifically at Lys40. We co-transfected HEK293 cells with *KAT2A* adenovirus and WT EGFP-TUBA plasmid, and acetylation-defective TUBA plasmid (EGFP-TUBA^{K40R}) [30]. Overexpression of *KAT2A* increased the acetylation of TUBA in the cells transfected with EGFP-WT-TUBA but not in the cells transfected

with mutant EGFP-TUBA^{K40R} (Figure 4K), supporting the notion that *KAT2A* acetylates Lys40 of TUBA.

Autophagy deficiency increases microtubule stability

Acetylation of TUBA is a well-established marker of more stable microtubules in cells [31]. We observed that autophagy regulated acetylated TUBA levels (Figure 1) and that suppression of autophagy by genetic deletion (*atg5*^{-/-} and *atg7*^{-/-} MEFs) or gene silencing (*ATG5*-, *ATG7*-, *BECN1*-, and *ULK1*-transfected HASMCs) increased the amount of acetylated TUBA (Figure 1E, G, I, and J). On the contrary, activation of autophagy by starvation with HBSS decreased TUBA acetylation (Figure 1F, H). We verified the effect of autophagy on acetylation of TUBA using immunofluorescence staining of

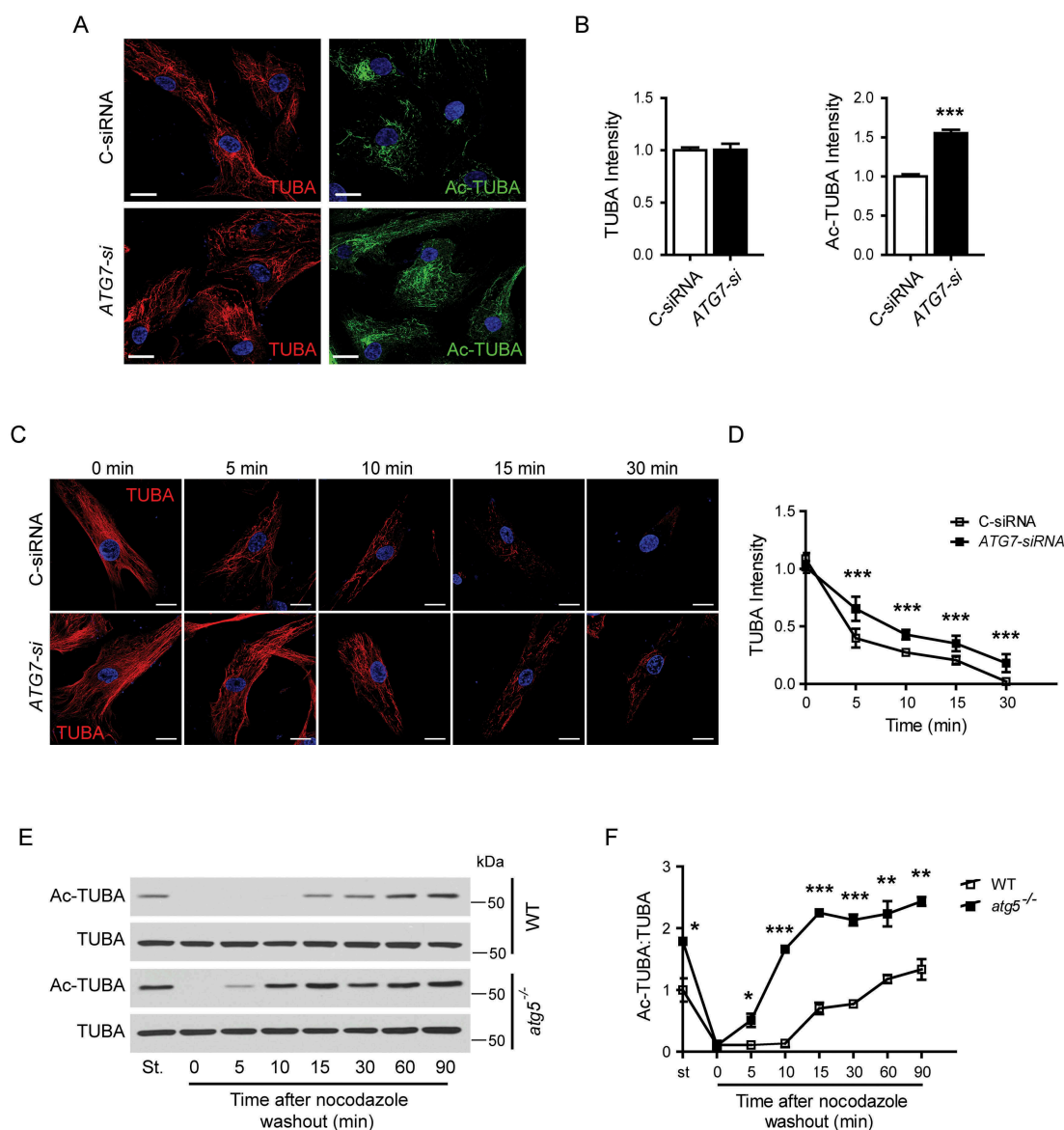


Figure 5. Autophagy deficiency increases microtubule stability. (A) HASMCs were transfected with control siRNA (C-siRNA) or *ATG7* siRNA (*ATG7*-si) for 48 h. TUBA and Ac-TUBA was stained by immunocytochemistry. Scale bar: 20 μ m. (B) Quantitative analysis of TUBA and Ac-TUBA intensity. $n = 3$, *** $P < 0.001$. (C) HASMCs transfected with C-siRNA or *ATG7*-si were incubated at 0°C for 0, 5, 10, 15, or 30 min. The morphology of microtubules was examined using immunostaining of TUBA and confocal microscope. Scale bar: 20 μ m. (D) Quantitative analysis of microtubule intensity. $n = 25$ /group, *** $P < 0.001$. (E) WT and *atg5*^{-/-} MEFs were treated with nocodazole for 30 min, and then the drug was washed out to allow the microtubules to repolymerize for the indicated times. Acetylation of TUBA (Ac-TUBA) in cell lysates were analyzed by western blot. St, steady-state situation without nocodazole treatment. (F) Densitometry analysis of acetylation of TUBA levels. $n = 3$, * $P < 0.05$, ** $P < 0.01$, *** $P < 0.001$.

acetylated TUBA in HASMCs transfected with *ATG7* siRNA (Figure 5A, B), compared with control siRNA treatment, *ATG7* siRNA transfection significantly increased the abundance of acetylation of TUBA (Figure 5A, B) but had no effect on the abundance of total TUBA. These effects on TUBA acetylation, therefore, suggest that autophagy negatively regulates microtubule stability.

We further determined the effect of autophagy on microtubule stability by examining the morphology of microtubules using immunofluorescence microscopy. HASMCs were transfected with control or *ATG7* siRNA and then incubated the cells at 0°C for 5, 10, 15 or 30 min. As shown in Figure 5C, D, cold treatment resulted in the depolymerization of microtubules in a time-dependent manner and microtubules were completely depolymerized after 30 min of cold treatment. In contrast, microtubules were still present in cells transfected with *ATG7* siRNA (Figure 5C, D). These data suggest that inhibition of autophagy increased microtubule stability.

To investigate whether autophagy deficiency affects microtubule assembly, we treated both WT and *atg5*^{-/-} MEFs with nocodazole (0.5 μM) for 30 min to depolymerize microtubules, the drug was then washed out to allow re-polymerization of microtubules. Western blot analysis revealed that K40-acetylated TUBA was barely detectable in WT and *atg5*^{-/-} MEFs following nocodazole treatment compared to levels in untreated MEFs; however, the acetylated TUBA levels recovered more quickly in *atg5*^{-/-} MEFs than in WT cells (Figure 5E, F), suggesting that autophagy deficiency promotes microtubule reassembly after nocodazole washout.

KAT2A-mediated acetylation of TUBA increases microtubule reassembly

Since defective autophagy resulted in KAT2A accumulation and KAT2A induced TUBA acetylation, a marker of microtubule stabilization, we assessed whether KAT2A regulates microtubule reassembly. To this end, we transfected HASMCs with adenovirus encoding Flag-KAT2A or GFP for 48 h and then treated the cells with nocodazole for 30 min to depolymerize microtubules. Tubulin acetylation was assessed by western blot and immunofluorescence microscopy after removal of nocodazole. The results showed that autophagy deficiency results in KAT2A accumulation (Figure 6A, B), overexpression of KAT2A in HASMCs promoted the recovery of acetylated TUBA protein levels following nocodazole washout (Figure 6A, B). Consistently, immunofluorescence analysis indicated a substantial amount of acetylated TUBA in HASMCs overexpressed KAT2A (Figure 6C, D). On the contrary, KAT2A silencing reduced acetylated TUBA protein levels under basal conditions and delayed the recovery of acetylated TUBA protein levels after nocodazole washout (Figure 6E, F). Collectively, KAT2A-induced TUBA acetylation increases microtubule reassembly under autophagy-deficient conditions.

Autophagy controls the directional migration of VSMCs

As autophagy dynamically modulates microtubule stability, which is an essential requirement for directional cell migration

[32], we examined the role of the autophagy-KAT2A-TUBA acetylation axis in cell polarization and subsequent cell migration. We first examined the effect of autophagy inhibition on cell polarity using the scratch wound healing assay. We found that inhibition of autophagy by *ATG7* siRNA interfered with microtubule-organizing center (MTOC) reorientation in the leading cells (Figure 7A, B), as evidenced by larger angles (θ) in *ATG7* siRNA-treated cells relative to those of control siRNA-treated cells. In addition, in control siRNA-treated HASMCs, the first two layers of leading cells were clearly polarized toward the leading edge, as shown via staining of the stabilized microtubules with acetylated-TUBA antibody. Inhibition of autophagy by *ATG7* silencing, however, dramatically increased the level of stable microtubules in the first two layers of leading cells and resulted in a loss of orientation toward the leading edge in these cells (Figure 7C).

Finally, we tested the effect of autophagy on HASMC migration. In the scratch wound healing assay, control siRNA-treated cells migrated into the wound area and organized a dense cellular network, resulting in nearly complete wound recovery after 48 h, while siRNA silencing of either *ATG7* or *BECN1* significantly inhibited cell migration into the wound area (Figure 7D, E). The transwell assay also showed that transfection of HASMCs with *ATG7* or *BECN1* siRNA drastically reduced cell migration through the filter membrane (Figure 7F, G). Conversely, adenoviral overexpression of ATG5 or ATG7 significantly promoted cell migration into the wound areas (Figure 7H, I) and significantly increased the numbers of HASMCs that migrated through the filter membrane (Figure 7J, K). These data suggest that autophagy is required to establish front-rear polarity and proper cell migration, presumably through the regulation of microtubule acetylation and stabilization.

KAT2A is required for autophagy regulation of VSMC migration

To determine whether KAT2A-acetylated TUBA mediated autophagy-regulated cell migration, we first examined whether KAT2A regulates cell migration. We transfected HASMCs with control or *KAT2A* siRNA and found that *KAT2A* silencing (Figure 8A) promoted cell migration into the wound areas in the scratch wound healing assay (Figure 8B, C). Conversely, adenoviral overexpression of KAT2A inhibited cell migration through the membrane in the transwell assay (Figure 8D–F). We then co-transfected HASMCs with *ATG7* and *KAT2A* siRNA and examined cell migration. Transfection of *ATG7* siRNA reduced ATG7 protein expression and concomitantly increased protein levels of KAT2A and acetylated TUBA. Administration of *KAT2A* siRNA prevented *ATG7* siRNA-enhanced acetylation of TUBA (Figure 8G). Notably, *ATG7* silencing inhibited VSMCs migration into the wound area, while *KAT2A* silencing promoted this VSMC migration. The observed inhibition of VSMCs migration attained by *ATG7* silencing was attenuated by silencing of *KAT2A* (Figure 8H, I).

To establish links between KAT2A, TUBA acetylation, and VSMCs migration, we co-transfected HASMCs with *KAT2A* adenovirus and WT TUBA plasmid or with *KAT2A* adenovirus and a dominant negative Lys40 acetylation-defective

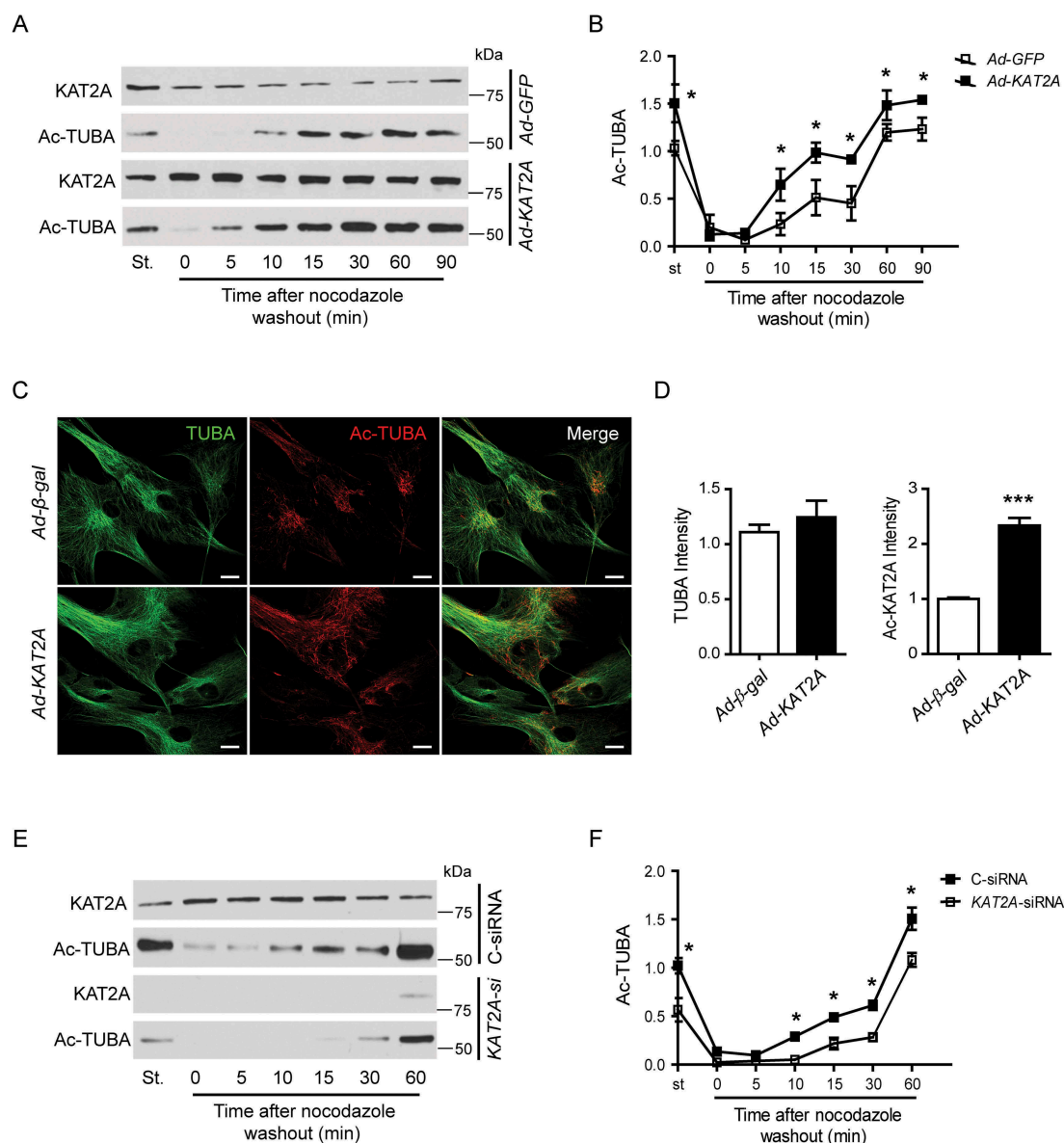


Figure 6. KAT2A-mediated acetylation of TUBA increases microtubule reassembly. (A) HASMCs were transfected with adenovirus encoding GFP and KAT2A. Cells were treated with nocodazole for 30 min, and then the drug was washed out to allow the microtubules to repolymerize for the indicated times. Cell lysates were analyzed by western blot. St, steady-state situation without nocodazole treatment. (B) Densitometry analysis of acetylated TUBA level. $n = 3$, $*P < 0.05$. (C) HASMCs were transfected with adenovirus encoding β -gal or KAT2A for 48 h, and acetylation of TUBA was measured using immunofluorescence. Scale bar: 20 μ m. (D) Quantitative analysis of TUBA and Ac-TUBA intensity. $n = 3$, $***P < 0.001$. (E) HASMCs were transfected with control siRNA (C-siRNA) or KAT2A-siRNA (KAT2A-si), and cells were subjected to the nocodazole-washout assay as described. (F) Densitometry analysis of acetylated TUBA levels. $n = 3$, $*P < 0.05$.

TUBA plasmid (TUBA^{K40R}) [30]. In the cells transfected with WT TUBA, overexpression of KAT2A reduced the numbers of cells that migrated through the membrane compared with overexpression of GFP. Transfection of cells with the TUBA^{K40R} mutant, however, significantly prevented KAT2A-induced reduction in VSMCs migration (Figure 8J, K). Together, these findings indicate that KAT2A-mediated acetylation of TUBA is required for defective autophagy inhibition of VSMC migration.

Discussion

In this study, we showed that selective autophagic degradation of histone acetyltransferase KAT2A controls cell migration by

regulating microtubule stability. KAT2A binds directly to the autophagic effector protein LC3 via an LIR motif, which mediates autophagic degradation of KAT2A. Suppression of autophagy resulted in KAT2A accumulation, and KAT2A-induced TUBA acetylation increased microtubule stability, leading to an inhibition of cell migration. Together, our results demonstrate that autophagy controls microtubule stability by regulating KAT2A protein expression.

Although autophagy has been considered a nonspecific degradation process, recent studies demonstrated that autophagy is also critical for the degradation of specific cargo, such as organelles and proteins [13,33,34]. In agreement with these findings, we observed that inhibition of autophagy led to an increase in KAT2A protein levels but had no effect on KAT2A

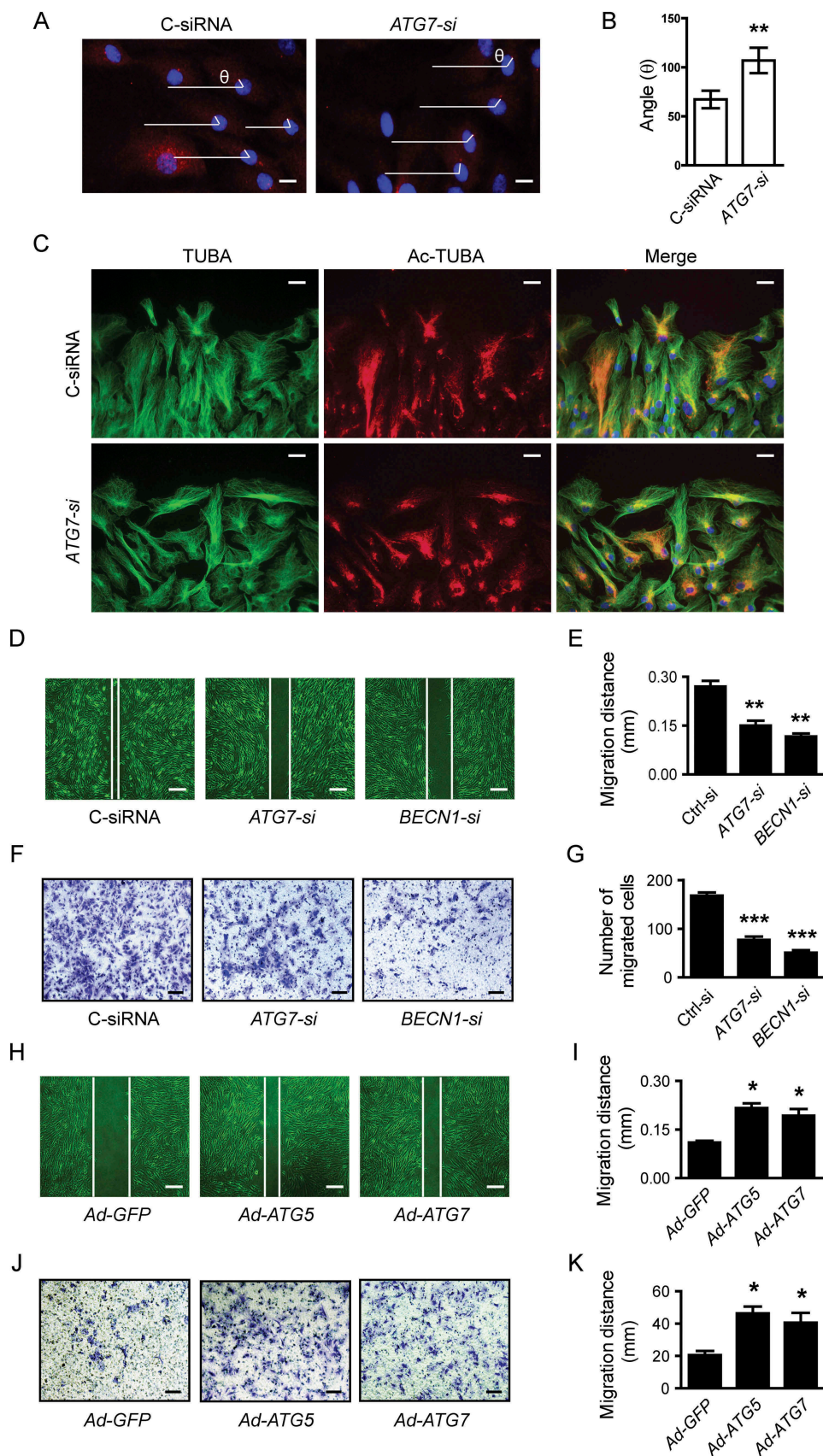


Figure 7. Autophagy is required for polarization and directional migration of VMSCs *in vitro*. (A) Representative images of HASMCs stained with TUBG antibody in cells subjected to a scratch wound assay. The cells were treated with control siRNA or *ATG7* siRNA for 48 h, and the images were captured 6 h after the scratch. Scale bar: 20 μ m. The cell polarization was assessed by the angles (θ) between the lines of TUBG and the scratched line at the center of each nucleus as a marker for microtubule-organizing center (MTOC) reorientation. (B) Quantitation of the angles (θ). $n = 100$, $*P < 0.01$ vs. C-siRNA. (C) Images of HASMC stained with TUBA (green) and Ac-TUBA (red) antibodies in cells subjected to the scratch wound assay. Nuclei were stained with DAPI (blue). The cells were transfected with control siRNA (C-siRNA), *ATG7* siRNA (*ATG7*-si), or *BECN1* siRNA (*BECN1*-si) for 48 h. (D) Representative images of HASMC migration in the scratch wound assay. Scale bar: 1 mm. (E) Migration distances of HASMCs. $n = 4$, $**P < 0.01$ vs. C-siRNA. (F) Cell migration was determined by transwell migration assays. Scale bar: 1 mm. (G) Migrated cells were quantified. $n = 5$, $***P < 0.001$ vs. C-siRNA. (H-K) HASMCs were transfected with adenovirus encoding GFP, ATG5, or ATG7 for 48 h. (H) Representative images of HASMC migration in the scratch wound assay. Scale bar: 1 mm. (I) Migration distances of HASMCs. $n = 4$, $*P < 0.05$ vs. C-siRNA. (J) Cell migration was determined by transwell migration assays. Scale bar: 1 mm. (K) Migrated cells were quantified. $n = 4$, $*P < 0.05$ vs. C-siRNA.

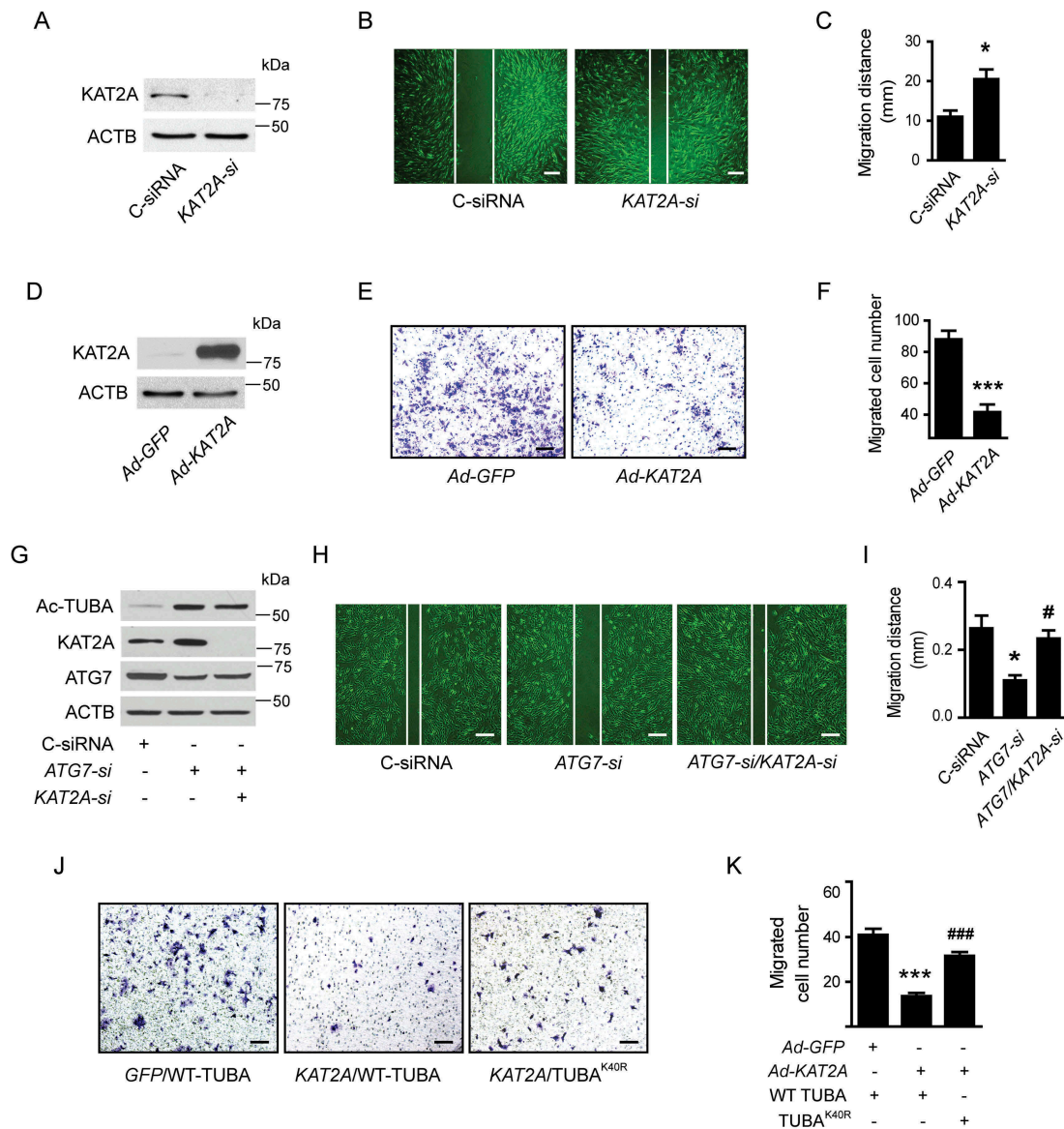


Figure 8. KAT2A inhibits VSMC migration by acetylating TUBA. (A-C) HASMCs were transfected with control siRNA (C-siRNA) or KAT2A-siRNA (KAT2A-si) for 48 h. (A) KAT2A levels were analyzed by western blot. (B) Representative images of HASMC migration in the scratch wound assay. Scale bar: 1 mm. (C) Migration distances of HASMCs. $n = 4$, * $P < 0.05$ vs. C-siRNA. (D-F) HASMCs were transfected with Ad-GFP or Ad-KAT2A for 48 h. (D) Levels of KAT2A were analyzed by western blotting. (E) Cell migration was determined by transwell migration assays. Scale bar: 1 mm. (F) Migrated cells were quantified. $n = 5$, * $P < 0.05$ vs. C-siRNA. (G-I) HASMCs were transfected with control siRNA (C-siRNA), ATG7 siRNA, or ATG7 and KAT2A siRNA for 48 h. (G) Levels of acetylated TUBA (Ac-TUBA), KAT2A, and ATG7 in cell lysates were measured by western blotting. (H) Representative images of HASMC migration in the scratch wound assay. Scale bar: 1 mm. (I) Migration distances of HASMCs. $n = 3$, * $P < 0.05$ vs. C-siRNA. # $P < 0.05$ vs. ATG7-siRNA. (J) HASMCs were co-transfected with Ad-GFP/WT TUBA, Ad-KAT2A/WT TUBA, or Ad-KAT2A/TUBA^{K40R} mutant for 48 h. Cell migration was determined by transwell migration assays. Scale bar: 1 mm. (K) Migrated cells were quantified. $n = 5$, *** $P < 0.001$ vs. Ad-GFP/WT TUBA; ### $P < 0.001$ vs. Ad-KAT2A/WT TUBA.

mRNA expression, whereas activation of autophagy reduced KAT2A protein expression and administration of a proteasome inhibitor had no effect on KAT2A protein expression. In addition, KAT2A contains an LIR motif, which mediates the association between KAT2A and LC3, recruiting KAT2A to autophagosomes. Deletion of the LIR motif prevented the degradation of KAT2A by starvation-induced autophagy. These data indicate that KAT2A is selectively degraded through the autophagy-lysosomal pathway and that the interaction between KAT2A and LC3 via the LIR motif is required for degradation of KAT2A by autophagy.

SQSTM1 has been proposed to contribute to selective autophagy of protein aggregates and depolarized mitochondria [35]. Thus, we investigated whether SQSTM1 is required for KAT2A degradation by autophagy. Although LC3 bound to SQSTM1 and KAT2A separately, KAT2A was not associated with SQSTM1. Importantly, gene silencing of SQSTM1 did not disrupt the association between KAT2A and LC3, indicating that SQSTM1 is not involved in the interaction between KAT2A and LC3 and that direct binding between KAT2A and LC3 mediates autophagic degradation of KAT2A.

Tubulin acetylation was first described 20 years ago, but little is known about the enzymes that catalyze this reaction.

Recent evidence suggests that *Atat1/atat-2* may function as the major TUBA acetyltransferase in *C. elegans* [36] and mice [37]. In *C. elegans*, loss of *atat-2* leads to disruption of microtubule structural integrity and axonal morphologic defects in touch receptor neurons [38]. In mice, ATAT1 is highly expressed in testis, kidney, and brain [37], the loss of ATAT1 results in brain abnormalities [37] and abnormal sperm morphology and motility [39]. Because neither activation nor suppression of autophagy alters ATAT1 expression, it is unlikely that autophagy via ATAT1 regulates TUBA acetylation in our system.

In the current study, we demonstrated that KAT2A is the enzyme that mediates acetylation of TUBA in VSMCs. The following lines of evidence support this conclusion: co-immunoprecipitation indicated that KAT2A physically associates with TUBA, immunofluorescence analysis revealed that endogenous KAT2A colocalized with acetylated TUBA, and an *in vitro* tubulin acetylation assay showed that full-length recombinant KAT2A induces acetylation of TUBA. Furthermore, KAT2A silencing decreased TUBA acetylation, while overexpression of KAT2A increased TUBA acetylation. Importantly, overexpression of KAT2A increased acetylation of WT-TUBA but failed to induce acetylation of TUBA^{K40R} mutant, in which Lys40 was substituted with arginine [30]. Thus, KAT2A represents a newly described acetyltransferase that targets TUBA. KAT2A, which is first identified as a global coactivator, and transcription-related histone acetyltransferase [40], has been reported to be involved in a broad range of cellular processes including gene transcription, differentiation, DNA repair, nucleosome assembly, and cell cycle regulation [41]. Although our results strongly indicate suggests that KAT2A directly acetylates TUBA, we cannot exclude that it can indirectly regulates TUBA acetylation via other molecules. Deacetylation of TUBA is mediated by both HDAC6 and SIRT2 [7,8]; however, the increased acetylation of TUBA in autophagy-deficient conditions may not be mediated by either of these deacetylases because neither activation nor suppression of autophagy alters the expression of HDAC6 or SIRT2.

The extent and duration of autophagy are crucial for cell health, and acute and chronic manipulations of autophagy have led to, in several instances, controversial conclusion. Our results are consistent with the findings that induction of autophagy is coupled to reduction of H4K16ac [19], and α -lipoic acid inhibits cellular autophagic flux and promotes the rapid hyperacetylation of TUBA [42]. However, other groups also showed that nutritional stress triggers hyperacetylation of tubulin in HeLa cells by an unidentified mechanism [43], and voluntary exercise increases acetylated tubulin levels, associated with activation of autophagy in mutated CRYAB^{R120G} (CryABR120G) transgenic mouse hearts [44].

Accumulating evidence suggests that microtubules regulate autophagosome formation and transportation in axon [45,46]. Whether autophagy in turn modulates microtubule stability in VSMCs is not known. In the present study we found that suppression of autophagy resulted in KAT2A accumulation, and KAT2A-induced TUBA acetylation increased microtubule stability, leading to an inhibition of cell migration. This finding is consistent with the report that inhibition of the

HDAC6 by siRNA or tributyrin increased tubulin acetylation and inhibited endothelial cell migration [47]. However the role of autophagy on microtubule stability seems to be different in different cell types, because a recent study showed that activation of autophagy increases microtubule stability through the degradation of STMN2 (stathmin 2), a microtubule destabilization protein, and promotes axon regeneration after spinal cord injury [48]. STMN2 is a neuron-specific, membrane-associated protein that is highly concentrated in growth cones of developing neurons. Thus, further investigations are warranted to determine the role of autophagy on microtubule stability in different cell types.

Microtubule stability plays important roles in autophagy. Treatment of cells with nocodazole leads to complete depolymerization of both labile and stable microtubules and fully inhibits autophagic flux. Autophagosome formation is also inhibited by treatment with taxol, a drug that stabilizes microtubules and interferes with the dynamic turnover of the microtubule network [49]. It is now clear that microtubules are involved in autophagosome formation [50]. First, microtubules interact with ATG proteins, including LC3, ULK1, BECN1, ATG5, and ATG12, supporting the assembly of pre-autophagosomal structure [51]. Second, microtubules regulate two major complexes (MTORC1 and PtdIns3K complex) [51] involved in the initiation of autophagy. In VSMCs, activation of autophagy results in destabilization of microtubules, which may inhibit the interaction between microtubules and ATG proteins and prevent the formation of initiation complexes, MTORC1 and PtdIns3K complex, therefore tuning down autophagy.

The role of TUBA acetylation on microtubule stability has been controversial. Early studies indicated that TUBA acetylation had no effect on microtubule polymerization [52]; however, more recent studies reported that increased acetylation of TUBA by HDAC6 inhibition increases microtubule stability and inhibits cell motility [53,54]. Since HDAC6 may regulate many other proteins in addition to TUBA, it has been difficult to determine whether these results are direct effects of HDAC6-mediated deacetylation of microtubules or indirect effects via other molecules. In our study, we found that KAT2A induced TUBA acetylation and dose-dependently increased microtubule polymerization. Overexpression of KAT2A protected microtubules from nocodazole-induced depolymerization, supporting the notion that acetylation of TUBA stabilizes microtubules. We also observed that KAT2A silencing increased cell migration into the wound area in a scratch wound healing assay. Overexpression of KAT2A inhibited cell migration in cells transfected with WT TUBA, but transfection of cells with the TUBA^{K40R} mutant significantly attenuated this KAT2A-induced inhibition of VSMC migration, suggesting that KAT2A-mediated acetylation of TUBA inhibits cell migration. However, the role of stabilized microtubules in migration is greatly understudied. It has been reported that reduced TUBA acetylation impairs migration in neuronal cell lines [5,55], and in breast cancer cells [56]. Conflicting reports have suggested that HDAC inhibitors, specifically targeting HDAC6's tubulin deacetylase activity, reduces cancer migration by increasing TUBA acetylation in estrogen

receptor-positive breast cancer [57], in addition, enhanced acetylated TUBA decreased cell motility in a human non-small cell lung carcinoma cell line (H1299) and NIH 3T3 fibroblasts [8,58]. Moreover, hyperacetylation of tubulin suppressed cell migration in endothelial cells [47]. Our results suggest that acetylation of TUBA increases microtubule stability and inhibits cell motility in VSMCs.

Recent studies have clearly demonstrated that autophagy has a greater variety of physiological and pathophysiological roles, including starvation adaptation, intracellular protein and organelle clearance, elimination of microorganisms, and antigen presentation [34,59,60]. We further demonstrated that autophagy regulates microtubule dynamics and cell motility through modulating TUBA acetylation. The role of autophagy in regulation of VSMC migration remains a subject of debate in the literature. Consistent with our findings, both PDGF-BB and 1-palmitoyl-2-(5-oxovaleryl)-sn-glycero-3-phosphocholine (POVPC) induce autophagy and concomitantly promote the loss of contractile gene expression and increase cell proliferation and migration [61,62]. By contrast, administration of the autophagy inducer rapamycin inhibits cell proliferation and prevents restenosis after angioplasty [63,64]. These effects of rapamycin are unlikely due to its activation of autophagy [62]. Rather, the drugs appear to prevent proliferation and migration by inhibiting RPS6KB1/S6K1 (ribosomal protein S6 kinase, polypeptide 1) [65,66] and regulating the expression of key cell cycle protein CDKN1B/p27^{Kip1} [67]. Intriguingly, rapamycin promotes Schwann cell migration via unidentified mechanisms [68]. Another study demonstrated that VSMC-specific deletion of *ATG7* accelerates senescence and promotes neointimal formation and atherogenesis [18]. One explanation for this discrepancy is that autophagy can also occur in the absence of some key autophagy proteins, such as *ATG5* and *ATG7*, through unconventional biogenesis of canonical autophagosomes [23]. In addition, *ATG7* has been reported to regulate TRP53/p53-dependent cell cycle and cell death pathways independent of autophagy during metabolic stress [69]. Thus, further investigation is necessary to determine the role of autophagy in regulating VSMC migration. A mouse with VSMC-specific deletion of *ULK1*, a protein essential for regulating both *ATG5/ATG7*-dependent and *ATG5/ATG7*-independent autophagy [23], may be useful for these investigations.

In conclusion, *KAT2A* is the acetyltransferase responsible for acetylation of TUBA and is selectively degraded by the autophagy-lysosomal pathway. Stabilization of microtubules by *KAT2A*-mediated acetylation of TUBA is an important mechanism by which defective autophagy inhibits VSMC migration. Our findings suggest that autophagy suppression in VSMCs may be an important therapeutic target for atherosclerosis and intimal hyperplasia.

Materials and methods

Reagents

Antibodies and reagents are from the following companies: *ATG5* (Cell Signaling Technology, 8540), *ATG7* (Cell Signaling

Technology, 8588), *SQSTM1/p62* (abcam, 56416), *BECN1* (Cell Signaling Technology, 3738), *TUBA/α-Tubulin* (Cell Signaling Technology, 3873), *MAP1LC3A/B* (Cell Signaling Technology, 4108), *ULK1* (Cell Signaling Technology, 8054), *KAT2A/GCN5* (abcam, 137515), acetylated-lysine (Cell Signaling Technology, 9441), *MYC-tag* (Cell Signaling Technology, 2276), *HDAC6* (Cell Signaling Technology, 7612), *SIRT1* (Cell Signaling Technology, 9475), mouse secondary antibody (Cell Signaling Technology, 7076), rabbit secondary antibody (Cell Signaling Technology, 7074), *ACTB/β-actin* (Santa Cruz Biotechnology, 47778), *EP300* (Santa Cruz Biotechnology, 48343), *GAPDH* (Santa Cruz Biotechnology, 32233), *Flag* (Sigma-Aldrich, 7425), *GFP* (Sigma-Aldrich, 1544), goat anti-mouse IgG conjugated to Alexa Fluor 594 red (ThermoFisher Scientific, 11032), goat anti-rabbit IgG conjugated to Alexa Fluor 555 red (ThermoFisher Scientific, 21434), anti-TUBA (Acetyl K40) antibody [6-11B-1] (abcam, 24610). *EnVision® + Dual Link System-HRP (DAB+)* (Dako Cytomation, 3468). The recombinant *KAT2A/GCN5*-catalytic domain (362--837) protein (Active Motif, 31204). Purified porcine brain tubulin protein (>99% pure) (Cytoskeleton Inc., T240). Recombinant human *GST-LC3* protein and *GST* protein (Enzo Life Sciences, BML-UW1195-0500). *KAT2A/GCN5* siRNA (Santa Cruz Biotechnology, 37946), *ULK1* siRNA (Santa Cruz Biotechnology, 44849), *ATG7* siRNA (Cell Signaling Technology, 6604), *ATG5* siRNA (Cell Signaling Technology, 6345), *SQSTM1* siRNA (Cell Signaling Technology, 6399). The siRNA delivery reagent Lipofectamine RNAiMAX (Life Technologies, 13778150), Lipofectamine® 2000 (Life Technologies, 11668019). Nocodazole (Sigma-Aldrich, 31430), chloroquine (Sigma-Aldrich, 6628), lactacystin (Sigma-Aldrich, 6785).

Plasmids and construction

Plasmids were obtained from Addgene: *EGFP-TUBA WT* (30487, Tso-Pang Yao's lab), *EGFP-TUBA^{K40R}* (64059, Weiping Han's lab), *MYC-LC3* (24919, Toren Finkel's lab), *EGFP-LC3* (11546, Karla Kirkegaard's lab). *Flag-KAT2A* plasmid was a gift from Dr. Ezra Burstein (Internal Medicine, UT Southwestern Medical Center). To identify the interaction between *LC3* and *KAT2A*, a series of *KAT2A* deletion was constructed by site-directed mutagenesis using a QuikChange II Kit (Stratagene, La Jolla, CA) according to the manufacturer's protocol. The primers used for the deletions were as follows: *KAT2AΔ1* (deletion of 661 bp–664 bp) forward 5'-gcatcccccccacatcatca -3', reverse 5'-gcatcccccccacatcatca -3'; *KAT2AΔ2* (deletion of 716 bp–719 bp) forward 5'-agagacaggcggaaggagaagggga -3', reverse 5'-tcccgcctgtctctcgaatgcag -3'; *KAT2AΔ3* (deletion of 734 bp–737 bp) forward 5'-cgaccagctcaaaaacctgctg -3', reverse 5'-gtttttgagctgtgctgggtccttcagc -3'; *KAT2AΔ4* (deletion of 826 bp–829 bp) forward 5'-agtcttcaaggaggaggcctcat -3', reverse 5'-ccctcctgaagaactcttcaggcgctg -3'. In addition, a double-site-mutant (*Y734A, L737A*) was constructed by multiple site-directed mutagenesis using QuikChange Multi Site-Directed Mutagenesis Kit (#200514, Agilent Technologies) according to the manufacturer's protocol with the following primers: 5'-cagctcgccaaccgcaaaaacctg-3' and 5'-gtttttggcggtgtggcgagctgtgctg-3'. All plasmids were confirmed by sequencing.

Cell culture and transfection

The *atg5*^{-/-} and *atg7*^{-/-} mouse embryonic fibroblasts (MEFs) were a kind gift from Dr. Masaaki Komatsu (The Tokyo Metropolitan Institute Medical Science, Tokyo, Japan). MEFs, HEK293 (ATCC, CRL-1573), and HeLa (ATCC, CCL-2) cells were maintained in Dulbecco's Modified Eagle's Media (DMEM) (Corning, 10-017-CV), supplemented with 10% fetal bovine serum (FBS) (Sigma, F0926). Human aortic smooth muscle cells (HASMCs) was purchased from Invitrogen (Life Technologies, C-007-5C) and maintained in Medium 231 (ThermoFisher Scientific, M231500) supplemented with 5% smooth muscle cell growth supplements (Sciencell, 1152). During the migration experiment, HASMCs were cultured in complete DMEM medium. All culture media were supplemented with penicillin (100 U/ml) and streptomycin (100 µg/ml) (ThermoFisher Scientific, 15140163). Cultured cells were incubated in a humidified atmosphere of 5% CO₂ and 95% ambient air at 37°C.

ATG5, *ATG7*, and *BECN1* siRNA were obtained from Cell Signaling. For siRNA depletion, HASMCs or MEFs were plated in 6-well plates. After reaching 70% confluence, the cells were treated with the indicated siRNA at a final concentration of 50 nM using Lipofectamine RNAiMAX reagent (Life Technologies, 13778150) in serum-free medium. After 6 h, the medium was removed and replaced with fresh medium containing 10% FBS. The cells were incubated in the fresh medium for 48 h. HeLa and HEK 293 cells were transfected with 2.5 µg plasmids using Lipofectamine 2000 (Life Technologies, 11668019). HASMCs and MEFs were electroporated with 2.5 µg plasmids using the 4D-Nucleofector™ System (Lonza, Frazer, PA, USA) according to the manufacturer's instructions. *ATG5* adenovirus was purchased from SignaGen Laboratories (Rockville, MD, USA). *ATG7* adenovirus was a gift from Dr. Jeffrey Robbins (Department of Pediatrics, The Cincinnati Children's Hospital Medical Center, Cincinnati, OH, USA). The adenoviruses encoding short hairpin *KAT2A* RNA (*sh-KAT2A*) or *KAT2A* were a gift from Dr. Pere Puigserver (Department of Cell Biology, Harvard Medical School, Boston, MA, USA). The adenoviruses were amplified in HEK293 cells and purified by CsCl₂ density gradient ultracentrifugation. Cells were infected with adenovirus at a multiplicity of infection of 100 for 2 h, and then medium was replaced with fresh normal medium. Protein expression was detected 48 h after transfection via immunoblotting analysis with specific antibodies.

Autophagy analysis

Autophagy activity was assessed by measuring GFP-LC3 puncta formation, LC3 cleavage, and SQSTM1 degradation. To determine autophagosome formation, cells were cultured on glass coverslips and allowed to adhere overnight. The cells were transfected with GFP-LC3 adenovirus for 24 h and then incubated with 5 µM chloroquine diphosphate (CQ) for another 24 h. After treatment, cells were fixed, and fluorescence images were obtained using a fluorescent microscope. Autophagy was measured by enumerating the average number of autophagosomes per cell for each sample. At least 100 cells per sample were counted.

Real-time PCR analysis

Total RNA was extracted from cultured cells using RNeasy Mini Kit (Qiagen, Valencia, CA). For reverse transcription, 1 µg of the total mRNA was converted to first-strand complementary DNA in 20 µL reactions using the iScript cDNA synthesis kit (Bio-Rad Laboratories, Hercules, CA). The primers used for amplification of genes were as follows: *KAT2A* (mouse) 5'-CGAGTTGTGCCGTAGCTGTGA-3' (forward) and 5'-ACCATCCCCAAGAGCCGGTTA-3' (reverse) and *GAPDH* (mouse) 5'-CCACTCCTCCACCTTTGAC-3' (forward) and 5'-ACCCTGTTGCTGTAGCCA-3' (reverse). Quantitative RT-PCR reactions were performed using *aiQ*™ SYBRGreen SupermixKit and a CFX96 real-time PCR detection system (Applied Biosystems, Foster City, CA) as described previously [70]. Calculations were performed using the comparative method (2-ΔΔCt) with *GAPDH* as an internal control [71].

Immunoprecipitation and immunoblotting

Immunoprecipitation (IP) was performed as described previously [72,73]. Briefly, cells were collected and lysed in RIPA buffer (10 mM Tris-HCl, pH 8.0, 1 mM EDTA, 140 mM NaCl, 0.1% SDS, 0.1% sodium deoxycholate, 1% Triton X-100; Sigma, R0278) containing a protease inhibitor cocktail (PI; Roche). Protein concentrations were measured with Pierce™ BCA Protein Assay Kit (ThermoFisher Scientific, 23225). After preclearing with protein A agarose beads (GE Healthcare, 17-0780-01) for 30 min at 4°C, whole-cell lysates were subjected to IP with the specific antibodies. Generally, 1 µg of antibody was added to 500 µg of cell lysate and incubated overnight at 4°C. After incubation with protein A agarose beads for 6 h, immunoprecipitates were eluted with SDS loading buffer by boiling for 10 min. The immunoprecipitated proteins were subjected to immunoblotting analysis.

For immunoblotting, cells were lysed in RIPA buffer containing a protease inhibitor cocktail as described previously [74,75]. Protein concentrations were measured with Pierce™ BCA Protein Assay Kit and lysates containing equal amounts of proteins were separated by SDS-PAGE and then transferred to nitrocellulose membranes. The membranes were blocked with 5% nonfat dry milk (LabScientific, M0841) and incubated with specific primary antibodies overnight at 4°C followed by secondary antibodies. All antibodies were used at the manufacturers' recommended dilutions. Immunoreactive bands were visualized by Super Signal™ West Pico PLUS chemiluminescent substrate (ThermoFisher, 34580) using an Odyssey scanner (LI-COR Biosciences, Bad Homburg, Germany) and Photoshop software. For quantification, the protein band intensities of the western blotting images were quantified with Alpha view software (ProteinSimple, San Jose, CA). Data are represented as mean intensity of bands from at least three independent experiments. The membranes were then stripped and probed for total protein and/or ACTB/β-actin to verify equal loading [74,75].

In vitro affinity-isolation assay

Glutathione S-transferase (GST) fusion proteins were immobilized on glutathione Sepharose 4 Fast Flow beads (GE Healthcare, 1707560) for 30 min at 4°C. For GST affinity isolation with purified His-tagged KAT2A protein, 4 µg of GST-LC3 protein was incubated with 1 µg of KAT2A protein in 500 µl of binding buffer (50 mM Tris-HCl, pH 8.0; 250 mM NaCl) for 120 min at 4°C and then washed 5 times with 1 ml of binding buffer. For GST affinity isolation in HeLa cell lysates, 4 µg of GST fusion proteins were incubated with 1,000 µg of HeLa cell lysate for 2 h at 4°C and then washed 5 times with 1 ml of lysis buffer. The precipitate complex was boiled with 2x Laemmli Sample Buffer (Bio-Rad) containing 1% SDS for 5 min at 95°C [76] and subjected to SDS-PAGE. After transfer to nitrocellulose membranes (Bio-Rad, 1620112), proteins were stained with Ponceau S (Sigma, P3504), followed by immunoblotting with the indicated antibodies.

In vitro tubulin acetylation assay

Purified porcine brain tubulin protein (>99% pure) was incubated with recombinant KAT2A-catalytic domain protein (362–837) protein in acetylation buffer (50 mM Tris, pH 8.0; 50 mM EDTA (Sigma, ED4SS); 10% glycerol; 20 µM acetyl CoA; 10 mM sodium butyrate (Sigma, B5887); 10 mM TSA (SELLECKCHEM, S1045); 1 mM GTP) at 37°C for 1 h. The acetylation of TUBA was assessed by western blotting.

Immunofluorescence

Cells were grown on glass coverslips, fixed with 4% paraformaldehyde for 15 min, and permeabilized with 0.2% Triton X-100 (Sigma, T8787) for 15 min. After blocking with goat serum, the cells were incubated with TUBA antibody (1:2000 dilution) and acetyl-TUBA antibody (1:300 dilution), followed by incubation with fluorescein conjugated secondary antibodies. Slides were mounted with Prolong Gold containing DAPI (Invitrogen) and analyzed with an Olympus microscope or LSM 510 Zeiss confocal microscope.

Microtubule depolymerization

The microtubule depolymerization experiments were performed as described previously [77]. Briefly, cells were incubated at 0°C for 5, 10, 15 or 30 min. The morphology of microtubules was then examined by immunostaining of TUBA and confocal microscope.

Nocodazole washout assay

To analyze nocodazole-induced microtubule depolymerization, cells were treated with 10 µM nocodazole for 30 min, and then the cells were washed with pre-warmed PBS (Sigma, D5652) and pre-warmed media and incubated in pre-warmed media without nocodazole for the indicated times. Cell lysates were analyzed by western blot using the indicated antibodies. In addition, cells grown on glass coverslips were incubated in

growth media with 10 µM nocodazole for 30 min, and then the drug was washed out to allow the microtubules to re-polymerize for the indicated times. The cells were fixed by immersion in ice-cold methanol and processed for immunofluorescence analysis.

Scratch wound healing assay

Monolayer smooth muscle cell migration was performed as described previously [78]. Briefly, HASMCs were plated on glass coverslips in 6-well plates at a concentration of 2.5×10^5 cells/well and transfected with either siRNA or adenovirus. Forty-eight hours later, a linear wound was gently made in the center of the confluent cell monolayer with a 200-µl pipette tip. The cells were then washed with fresh medium to remove the cellular debris. Repeated observations of the edge of the same scratched lesion were performed. After 10 h, images were captured using a microscope (IX71, Olympus) equipped with a digital camera. The distance of the gap closure was calculated as the total distance of the gap closed over the migration time. For analysis of cell polarity, the cells were fixed and immunostained with a TUBG/γ-tubulin antibody. The angles (θ) of each cell to the scratched line were measured as described by Nakano [76]. Briefly, line A was drawn from the point stained with a TUBG antibody to the center of the nucleus, line B was drawn from the center of the nucleus to the scratched line, and the angles (θ) between lines A and B were measured.

Transwell migration assay

Cell migration was examined using a transwell fitted with polycarbonate membrane (8-µm pore size, Corning Inc., Corning, NY). Briefly, growth-arrested HASMCs were trypsinized and resuspended at a concentration of 1×10^6 cells/ml in DMEM supplemented with 0.5% FBS. HASMC suspension (100 µl) was placed in the upper chamber, and 500 µl of DMEM containing 10% FBS was placed in the lower chamber. Cells were allowed to migrate through the pores of the membrane for 6 h at 37°C in the presence of 5% CO₂. The filter was then removed and fixed in 4% paraformaldehyde. The cells on the upper side of the filter were scraped off with a cotton swab, and the cells that migrated to the lower surface of the filter were stained with 0.2% Crystal violet (ThermoFisher Scientific, C581-100) in 10% methanol for 30 min. The chambers were washed thoroughly with water, and the cells on the lower surface of filters were counted using a light microscope. The experiments were performed at least three times in each group, and cell motility is presented as the number of migrated cells/field.

Statistical analysis

Data are presented as mean ± SEM. The differences between two groups were analyzed using the Student's *t*-test. Comparisons between multiple groups were performed using one-way analysis of variance (ANOVA) followed by Bonferroni post-hoc analysis. A value of *P* < 0.05 was considered statistically significant.

Acknowledgments

This study was supported by funding from the following agencies: NHLBI (HL079584, HL080499, HL089920, HL110488, HL128014, HL132500, HL137371, and HL142287), NCI (CA213022), NIA (AG047776), and AHA (16GRANT29590003). Dr. Zou is the Eminent Scholar in Molecular and Translational Medicine of the Georgia Research Alliance.

Disclosure statement

No potential conflict of interest was reported by the authors.

Funding

This work was supported by the American Heart Association [6GRANT29590003]; NIH [HL128014, HL132500, HL137371, and HL142287]; NIH [NHLBI (HL079584, HL080499, HL089920, HL110488, CA213022, and AG047776)].

References

- Kenagy RD, Fukai N, Min SK, et al. Proliferative capacity of vein graft smooth muscle cells and fibroblasts in vitro correlates with graft stenosis. *J Vasc Surg*. 2009 May;49(5):1282–1288.
- Schaper W, Ito WD. Molecular mechanisms of coronary collateral vessel growth. *Circ Res*. 1996 Nov;79(5):911–919.
- Etienne-Manneville S. Microtubules in cell migration. *Annu Rev Cell Dev Biol*. 2013;29:471–499.
- Mitchison T, Kirschner M. Dynamic instability of microtubule growth. *Nature*. 1984 Nov 15;312(5991):237–242.
- Creppe C, Malinouskaya L, Volvert ML, et al. Elongator controls the migration and differentiation of cortical neurons through acetylation of alpha-tubulin. *Cell*. 2009 Feb 6;136(3):551–564.
- Akella JS, Wloga D, Kim J, et al. MEC-17 is an alpha-tubulin acetyltransferase. *Nature*. 2010 Sept 9;467(7312):218–222.
- North BJ, Marshall BL, Borra MT, et al. The human Sir2 ortholog, SIRT2, is an NAD⁺-dependent tubulin deacetylase. *Mol Cell*. 2003 Feb;11(2):437–444.
- Hubbert C, Guardiola A, Shao R, et al. HDAC6 is a microtubule-associated deacetylase. *Nature*. 2002 May 23;417(6887):455–458.
- Chimal-Monroy J, Abarca-Buis RF, Cuervo R, et al. Molecular control of cell differentiation and programmed cell death during digit development. *IUBMB Life*. 2011 Oct;63(10):922–929.
- Sridhar S, Botbol Y, Macian F, et al. Autophagy and disease: always two sides to a problem. *J Pathol*. 2012 Jan;226(2):255–273.
- Cuervo AM. Autophagy: in sickness and in health. *Trends Cell Biol*. 2004 Feb;14(2):70–77.
- Kroemer G, Marino G, Levine B. Autophagy and the integrated stress response. *Mol Cell*. 2010 Oct 22;40(2):280–293.
- Kim PK, Hailey DW, Mullen RT, et al. Ubiquitin signals autophagic degradation of cytosolic proteins and peroxisomes. *Proc Natl Acad Sci U S A*. 2008 Dec 30;105(52):20567–20574.
- Popelka H, Klionsky DJ. Post-translationally-modified structures in the autophagy machinery: an integrative perspective. *Febs J*. 2015 Sept;282(18):3474–3488.
- Long L, Yang X, Southwood M, et al. Chloroquine prevents progression of experimental pulmonary hypertension via inhibition of autophagy and lysosomal bone morphogenetic protein type II receptor degradation. *Circ Res*. 2013 Apr 12;112(8):1159–1170.
- LaRocca TJ, Gioscia-Ryan RA, Hearon CM Jr., et al. The autophagy enhancer spermidine reverses arterial aging. *Mech Ageing Dev*. 2013 July;134(7–8):314–320.
- Martinet W, De Meyer GR. Autophagy in atherosclerosis: a cell survival and death phenomenon with therapeutic potential. *Circ Res*. 2009 Feb 13;104(3):304–317.
- Grootaert MO, da Costa Martins PA, Bitsch N, et al. Defective autophagy in vascular smooth muscle cells accelerates senescence and promotes neointima formation and atherogenesis. *Autophagy*. 2015;11(11):2014–2032.
- Fullgrabe J, Lynch-Day MA, Heldring N, et al. The histone H4 lysine 16 acetyltransferase hMOF regulates the outcome of autophagy. *Nature*. 2013 Aug 22;500(7463):468–471.
- Komatsu M, Waguri S, Ueno T, et al. Impairment of starvation-induced and constitutive autophagy in Atg7-deficient mice. *J Cell Biol*. 2005 May 9;169(3):425–434.
- Kuma A, Hatano M, Matsui M, et al. The role of autophagy during the early neonatal starvation period. *Nature*. 2004 Dec 23;432(7020):1032–1036.
- Mizushima N. Autophagy: process and function. *Genes Dev*. 2007 Nov 15;21(22):2861–2873.
- Nishida Y, Arakawa S, Fujitani K, et al. Discovery of Atg5/Atg7-independent alternative macroautophagy. *Nature*. 2009 Oct 1;461(7264):654–658.
- He C, Zhu H, Li H, et al. Dissociation of Bcl-2-Beclin1 complex by activated AMPK enhances cardiac autophagy and protects against cardiomyocyte apoptosis in diabetes. *Diabetes*. 2013;62:1270–81.
- Tomoda H, Omura S. Lactacystin, a proteasome inhibitor: discovery and its application in cell biology. *Yakugaku Zasshi*. 2000 Oct;120(10):935–949.
- Shen R, Wang X, Drissi H, et al. Cyclin D1-cdk4 induce runx2 ubiquitination and degradation. *J Biol Chem*. 2006 June 16;281(24):16347–16353.
- Suzuki H, Tabata K, Morita E, et al. Structural basis of the autophagy-related LC3/Atg13 LIR complex: recognition and interaction mechanism. *Structure*. 2014 Jan 7;22(1):47–58.
- Alemu EA, Lamark T, Torgersen KM, et al. ATG8 family proteins act as scaffolds for assembly of the ULK complex: sequence requirements for LC3-interacting region (LIR) motifs. *J Biol Chem*. 2012 Nov 16;287(47):39275–39290.
- Magiera MM, Janke C. Post-translational modifications of tubulin. *Curr Biol*. 2014 May 5;24(9):R351–R354.
- Dompierre JP, Godin JD, Charrin BC, et al. Histone deacetylase 6 inhibition compensates for the transport deficit in Huntington's disease by increasing tubulin acetylation. *J Neurosci*. 2007 Mar 28;27(13):3571–3583.
- Piperno G, LeDizet M, Chang XJ. Microtubules containing acetylated alpha-tubulin in mammalian cells in culture. *J Cell Biol*. 1987 Feb;104(2):289–302.
- Kaverina I, Straube A. Regulation of cell migration by dynamic microtubules. *Semin Cell Dev Biol*. 2011 Dec;22(9):968–974.
- Lu K, Psakhye I, Jentsch S. A new class of ubiquitin-Atg8 receptors involved in selective autophagy and polyQ protein clearance. *Autophagy*. 2014;10(12):2381–2382.
- Steele S, Brunton J, Kawula T. The role of autophagy in intracellular pathogen nutrient acquisition. *Front Cell Infect Microbiol*. 2015;5:51.
- Rogov V, Dotsch V, Johansen T, et al. Interactions between autophagy receptors and ubiquitin-like proteins form the molecular basis for selective autophagy. *Mol Cell*. 2014 Jan 23;53(2):167–178.
- Shida T, Cueva JG, Xu Z, et al. The major alpha-tubulin K40 acetyltransferase alphaTAT1 promotes rapid ciliogenesis and efficient mechanosensation. *Proc Natl Acad Sci U S A*. 2010 Dec 14;107(50):21517–21522.
- Kim GW, Li L, Ghorbani M, et al. Mice lacking alpha-tubulin acetyltransferase 1 are viable but display alpha-tubulin acetylation deficiency and dentate gyrus distortion. *J Biol Chem*. 2013 July 12;288(28):20334–20350.
- Topalidou I, Keller C, Kalebic N, et al. Genetically separable functions of the MEC-17 tubulin acetyltransferase affect microtubule organization. *Curr Biol*. 2012 June 19;22(12):1057–1065.
- Kalebic N, Sorrentino S, Perlas E, et al. alphaTAT1 is the major alpha-tubulin acetyltransferase in mice. *Nat Commun*. 2013;4:1962.

- [40] Kikuchi H, Barman HK, Nakayama M, et al. Participation of histones, histone modifying enzymes and histone chaperones in vertebrate cell functions. *Subcell Biochem.* **2006**;40:225–243.
- [41] Burgess RJ, Zhou H, Han J, et al. A role for Gcn5 in replication-coupled nucleosome assembly. *Mol Cell.* **2010** Feb 26;37(4):469–480.
- [42] Stoner MW, Thapa D, Zhang M, et al. alpha-Lipoic acid promotes alpha-tubulin hyperacetylation and blocks the turnover of mitochondria through mitophagy. *Biochem J.* **2016** June 15;473(12):1821–1830.
- [43] Geeraert C, Ratier A, Pfisterer SG, et al. Starvation-induced hyperacetylation of tubulin is required for the stimulation of autophagy by nutrient deprivation. *J Biol Chem.* **2010** July 30;285(31):24184–24194.
- [44] McLendon PM, Ferguson BS, Osinska H, et al. Tubulin hyperacetylation is adaptive in cardiac proteotoxicity by promoting autophagy. *Proc Natl Acad Sci U S A.* **2014** Dec 2;111(48):5178–5186.
- [45] Fu MM, Nirschl JJ, Holzbaue ELF. LC3 binding to the scaffolding protein JIP1 regulates processive dynein-driven transport of autophagosomes. *Dev Cell.* **2014** June 9;29(5):577–590.
- [46] Maday S, Wallace KE, Holzbaue EL. Autophagosomes initiate distally and mature during transport toward the cell soma in primary neurons. *J Cell Biol.* **2012** Feb 20;196(4):407–417.
- [47] Wang YH, Yan ZQ, Qi YX, et al. Normal shear stress and vascular smooth muscle cells modulate migration of endothelial cells through histone deacetylase 6 activation and tubulin acetylation. *Ann Biomed Eng.* **2010** Mar;38(3):729–737.
- [48] He M, Ding Y, Chu C, et al. Autophagy induction stabilizes microtubules and promotes axon regeneration after spinal cord injury. *Proc Natl Acad Sci U S A.* **2016** Oct 4;113(40):11324–11329.
- [49] Kochl R, Hu XW, Chan EY, et al. Microtubules facilitate autophagosome formation and fusion of autophagosomes with endosomes. *Traffic.* **2006** Feb;7(2):129–145.
- [50] Fass E, Shvets E, Degani I, et al. Microtubules support production of starvation-induced autophagosomes but not their targeting and fusion with lysosomes. *J Biol Chem.* **2006** Nov 24;281(47):36303–36316.
- [51] Mackeh R, Perdiz D, Lorin S, et al. Autophagy and microtubules - new story, old players. *J Cell Sci.* **2013** Mar 1;126(Pt 5):1071–1080.
- [52] Maruta H, Greer K, Rosenbaum JL. The acetylation of alpha-tubulin and its relationship to the assembly and disassembly of microtubules. *J Cell Biol.* **1986** Aug;103(2):571–579.
- [53] Matsuyama A, Shimazu T, Sumida Y, et al. In vivo destabilization of dynamic microtubules by HDAC6-mediated deacetylation. *Embo J.* **2002** Dec 16;21(24):6820–6831.
- [54] Tran AD, Marmo TP, Salam AA, et al. HDAC6 deacetylation of tubulin modulates dynamics of cellular adhesions. *J Cell Sci.* **2007** Apr 15;120(Pt 8):1469–1479.
- [55] Li L, Wei D, Wang Q, et al. MEC-17 deficiency leads to reduced alpha-tubulin acetylation and impaired migration of cortical neurons. *J Neurosci.* **2012** Sept 12;32(37):12673–12683.
- [56] Boggs AE, Vitolo MI, Whipple RA, et al. alpha-Tubulin acetylation elevated in metastatic and basal-like breast cancer cells promotes microtentacle formation, adhesion, and invasive migration. *Cancer Res.* **2015** Jan 1;75(1):203–215.
- [57] Saji S, Kawakami M, Hayashi S, et al. Significance of HDAC6 regulation via estrogen signaling for cell motility and prognosis in estrogen receptor-positive breast cancer. *Oncogene.* **2005** June 30;24(28):4531–4539.
- [58] Jung HY, Jung JS, Whang YM, et al. RASSF1A suppresses cell migration through inactivation of HDAC6 and increase of acetylated alpha-tubulin. *Cancer Res Treat.* **2013** June;45(2):134–144.
- [59] Mizushima N. The pleiotropic role of autophagy: from protein metabolism to bactericide. *Cell Death Differ.* **2005** Nov;12(Suppl 2):1535–1541.
- [60] Choi AM, Ryter SW, Levine B. Autophagy in human health and disease. *N Engl J Med.* **2013** May 9;368(19):1845–1846.
- [61] Salabei JK, Cummins TD, Singh M, et al. PDGF-mediated autophagy regulates vascular smooth muscle cell phenotype and resistance to oxidative stress. *Biochem J.* **2013** May 1;451(3):375–388.
- [62] Salabei JK, Hill BG. Implications of autophagy for vascular smooth muscle cell function and plasticity. *Free Radic Biol Med.* **2013** Dec;65:693–703.
- [63] Kim J, Kundu M, Viollet B, et al. mTOR and mTORC2 regulate autophagy through direct phosphorylation of Ulk1. *Nat Cell Biol.* **2011** Feb;13(2):132–141.
- [64] Jung CH, Ro SH, Cao J, et al. mTOR regulation of autophagy. *FEBS Lett.* **2010** Apr 2;584(7):1287–1295.
- [65] Martin KA, Merenick BL, Ding M, et al. Rapamycin promotes vascular smooth muscle cell differentiation through insulin receptor substrate-1/phosphatidylinositol 3-kinase/Akt2 feedback signaling. *J Biol Chem.* **2007** Dec 7;282(49):36112–36120.
- [66] Gallo R, Padurean A, Jayaraman T, et al. Inhibition of intimal thickening after balloon angioplasty in porcine coronary arteries by targeting regulators of the cell cycle. *Circulation.* **1999** Apr 27;99(16):2164–2170.
- [67] Sun J, Marx SO, Chen HJ, et al. Role for p27(Kip1) in vascular smooth muscle cell migration. *Circulation.* **2001** June 19;103(24):2967–2972.
- [68] Liu F, Zhang H, Zhang K, et al. Rapamycin promotes Schwann cell migration and nerve growth factor secretion. *Neural Regen Res.* **2014** Mar 15;9(6):602–609.
- [69] Lee IH, Kawai Y, Fergusson MM, et al. Atg7 modulates p53 activity to regulate cell cycle and survival during metabolic stress. *Science.* **2012** Apr 13;336(6078):225–228.
- [70] Tedesco L, Valerio A, Cervino C, et al. Cannabinoid type 1 receptor blockade promotes mitochondrial biogenesis through endothelial nitric oxide synthase expression in white adipocytes. *Diabetes.* **2008** Aug;57(8):2028–2036.
- [71] Pfaffl MW. A new mathematical model for relative quantification in real-time RT-PCR. *Nucleic Acids Res.* **2001** May 1;29(9):e45.
- [72] He C, Zhu H, Li H, et al. Dissociation of Bcl-2-Beclin1 complex by activated AMPK enhances cardiac autophagy and protects against cardiomyocyte apoptosis in diabetes. *Diabetes.* **2013** Apr;62(4):1270–1281.
- [73] Xie Z, Dong Y, Zhang J, et al. Identification of the serine 307 of LKB1 as a novel phosphorylation site essential for its nucleocytoplasmic transport and endothelial cell angiogenesis. *Mol Cell Biol.* **2009** July;29(13):3582–3596.
- [74] Zou MH, Li H, He C, et al. Tyrosine nitration of prostacyclin synthase is associated with enhanced retinal cell apoptosis in diabetes. *Am J Pathol.* **2011** Dec;179(6):2835–2844.
- [75] Xie Z, Singh M, Siwik DA, et al. Osteopontin inhibits interleukin-1beta-stimulated increases in matrix metalloproteinase activity in adult rat cardiac fibroblasts: role of protein kinase C-zeta. *J Biol Chem.* **2003** Dec 5;278(49):48546–48552.
- [76] Nakano A, Kato H, Watanabe T, et al. AMPK controls the speed of microtubule polymerization and directional cell migration through CLIP-170 phosphorylation. *Nat Cell Biol.* **2010** June;12(6):583–590.
- [77] Sun X, Shi X, Liu M, et al. Mdp3 is a novel microtubule-binding protein that regulates microtubule assembly and stability. *Cell Cycle.* **2011** Nov 15;10(22):3929–3937.
- [78] Liang CC, Park AY, Guan JL. In vitro scratch assay: a convenient and inexpensive method for analysis of cell migration in vitro. *Nat Protoc.* **2007**;2(2):329–333.